PH5CH8 cells revealed that NS3-4A (1B-1 strain) was still unable to cleave the TRIF mutants possessing D or E at the P6 position, even though an acidic aa (D or E) is known to be important for cleavage by NS3-4A [23] (Fig. 1b). Although we demonstrated that exogenously expressed Cardif, but not TRIF, was cleaved by NS3-4A (1B-1 or O strain) [6], no studies had determined whether endogenous Cardif or TRIF can be cleaved by NS3-4A. To clarify these issues, we selected anti-Cardif and anti-TRIF antibodies, and we immunoprecipitated lysates from PH5CH8 cells [in which NS3-4A (1B-1 or O strain) was overexpressed] and lysates from genome-length HCV RNA-replicating O cells [14]. We then performed immunoblot analyses using anti-Cardif, anti-TRIF, or NS3 antibodies. The results revealed that endogenous TRIF was also not cleaved by the NS3-4A expressed in PH5CH8 and O cells, whereas endogenous Cardif (75 kDa) was efficiently cleaved to the expected size (70 kDa) in PH5CH8 and O cells (Fig. 2a). On the other hand, we observed that NS3 interacted with TRIF, but not with Cardif, in both PH5CH8 and O cells (Fig. 2a), as had also been observed previously by another group [10]. In addition, we demonstrated that endogenous Cardif was cleaved by the NS3-4A/W1528A mutant, which lacks RNA helicase activity, but not by the NS3-4A/S1165A mutant, which lacks the serine protease activity (Fig. 2b). Furthermore, we examined whether or not endogenous Cardif and TRIF are cleaved in JFH-1-infected RSc cells. The results revealed that endogenous TRIF was also not cleaved in JFH-1-infected RSc cells, whereas endogenous Cardif was efficiently cleaved in these cells (Fig. 2c). In addition, we also observed that NS3 interacted weakly with TRIF, but not with Cardif, in these cells (Fig. 2c). We therefore concluded that endogenous TRIF is not cleaved by NS3-4A derived from at least the 1B-1 (genotype 1b), O (genotype 1b) or JFH-1 (genotype 2a) strain.

None of the NS3-4As derived from patients with different hepatic disease diagnoses prevented extracellular dsRNA-induced IFN-β transcription via the TRIF-mediated pathway

Although we demonstrated that NS3-4As derived from healthy carriers (1B-1 and O) was unable to suppress IFN-β production induced by the TRIF-mediated pathway [6], there is still no evidence that NS3-4As derived from patients with various hepatic disease diagnoses carry out such suppression. To obtain more evidence, we first amplified NS3-4A-encoding regions by RT-PCR using sera derived from five HCV-positive healthy carriers (including strains 1B-1 and O), one patient with acute hepatitis, seven patients with chronic hepatitis, and two patients with hepatocellular carcinoma; using these samples, we next constructed 15 types of NS3-4A expression vector. Although we observed that all of the NS3-4As expressed in PH5CH8 cells were processed into NS3 and NS4A by an intramolecular reaction, there were some size differences (60–65 kDa) of NS3 and NS4A (Fig. 3a). These size differences may be related to the aa sequence variation, as described below. Sequence analysis of these NS3-4A-encoding regions revealed that the aa sequences involved

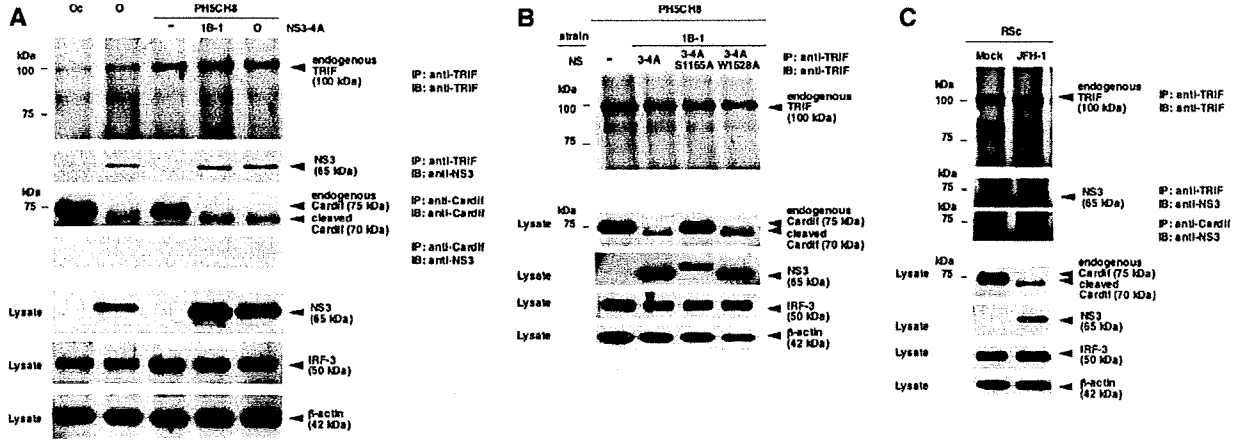

Fig. 2 NS3-4A lack the ability to cleave endogenous TRIF, but not Cardif. **a** Endogenous Cardif, but not TRIF is cleaved by NS3-4As from 1B-1 and O strains. Cell lysates were prepared and subjected to immunoprecipitation using anti-TRIF or anti-Cardif antibody. Bound proteins were collected from cell lysates using Protein G Sepharose and were subjected to immunoblot analysis using anti-TRIF, anti-Cardif, or anti-NS3 antibody. NS3, IRF3, and β-actin in the cell lysates were detected by anti-NS3, anti-IRF3, and anti-β-actin antibody, respectively. **b** Endogenous Cardif is cleaved by the serine protease activity of NS3-4A. The cell lysates were prepared and subjected to immunoprecipitation and followed by immunoblot analysis as described in **a**. **c** Endogenous Cardif, but not TRIF, is cleaved in JFH-1-infected RSc cells. The cell lysates were prepared and subjected to immunoprecipitation followed by immunoblot analysis as described in **a**

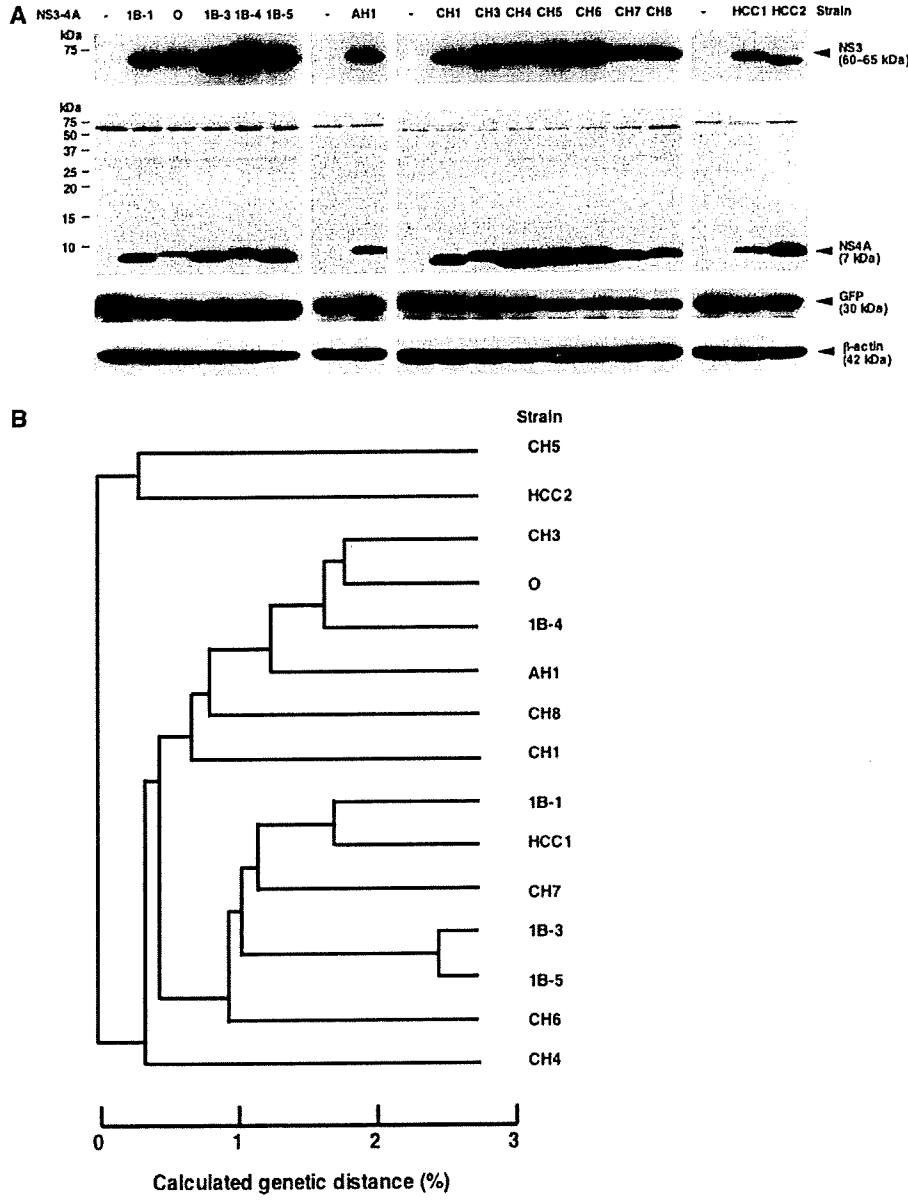

Fig. 3 Characterization of NS3-4As derived from patients with different hepatic disease diagnoses. **a** Expression of NS3 and NS4A in PH5CH8 cells. PH5CH8 cells were transfected with the expression vectors of NS3-4As derived from 15 different HCV strains and pEGFP-C1 (internal control reporter). Production of NS3 and NS4A in PH5CH8 cells was analyzed by immunoblot analysis using anti-NS3 and anti-NS4A antibody, respectively. PH5CH8 cells transfected with the pCX4bsr vector were used as a control (–). GFP was used to estimate the efficiency of transfection. β-actin was used as a control for the amount of protein loaded per lane. **b** Phylogenetic tree based on the amino acid sequences of NS3-4As used in this study

in the catalytic triad (H-57, D-81, and S-139), substrate recognition (L-135, F-154, A-157, and R-161), and metal coordination (C-97, C-99, C-145, and H-149) were well conserved among the NS3-4As (data not shown). In addition, the aa sequences (aa 626–631 in NS3, aa 1–5 in NS4A) surrounding the *cis*-cleavage site and aa 1–20 in NS4A, which is important for the stability of the NS3/4A complex, were also well conserved. The nucleotide sequences in the NS3-4 regions of these HCV strains showed differences of 6.62% (1B-4 strain)–10.47% (HCC2 strain) from those of the O strain. Similarly, the aa sequences in the NS3-4A regions of these HCV strains showed differences of 1.90% (CH3 strain)–5.11% (HCC2 strain) from those of the O strain. The phylogenetic tree based on the aa sequences of all NS3-4As examined is not indicative of any disease-stage-specific clusters (Fig. 3b).

Using these NS3-4A expression vectors, we examined the inhibitory effects of NS3-4As on dsRNA-induced IFN-β transcription in PH5CH8 cells. As described previously [6, 28], IFN-β transcription is induced via two pathways; one is mediated by the intracellular dsRNA (mainly the Cardif-mediated pathway), and the other is mediated by the extracellular dsRNA (TRIF-mediated pathway). Therefore, two different methods were used for the analysis, as described previously [6, 28]; one is to examine NS3-4A's inhibitory effects when the dsRNA

analog, poly(I-C), was introduced into cells using a liposome-mediated transfection procedure (the intracellular dsRNA, T-pIC), the other is to examine NS3-4A's inhibitory effects when poly(I-C) was added to the culture medium (the extracellular dsRNA, M-pIC). We observed that IFN-β gene promoter activity was strongly suppressed via the cleavage of Cardif by each NS3-4A when PH5CH8 cells were transfected with poly (I-C) (T-pIC) (Supplementary Fig. S1 in Electronic Supplementary Material). In contrast, IFN-β gene promoter activity was not significantly suppressed when poly (I-C) was added to the culture medium (M-pIC) (Fig. 4a). However, the promoter activity in cells expressing 1B-5-derived NS3-4A appeared to be slightly suppressed (Fig. 4a). Therefore, we next determined the levels of IFN-β mRNA by quantitative RT-PCR. The results revealed that IFN-β mRNA expression was not suppressed in cells expressing 1B-5-derived NS3-4A (Fig. 4b). We further showed that none of the NS3-4As examined cleaved the exogenously expressed TRIF (Fig. 4c). In addition, we showed that 1B-5, CH1, HCC1, or HCC2-derived NS3 interacted with endogenous TRIF, as was also observed with 1B-1-, O-, and JFH-1-derived NS3 (Figs. 2a, c, 4d). These results suggest that the suppressive effects of NS3-4As on dsRNA-induced IFN-β transcription and the interaction of NS3 with TRIF were not dependent on the HCV strain and genotype or associated with the stage or progression of hepatic disease.

Extracellular dsRNA-induced inflammatory cytokine production via the NF-κB signaling pathway was also not suppressed by NS3-4A

It was already known that TLR3-mediated IRF-3 and NF-κB activation pathways bifurcate at TRIF, and that TLR3 recruits TRAF6 via TRIF through the TRAF6-binding site of TRIF, resulting in NF-κB activation [17, 34]. Since we demonstrated that NS3 interacts with TRIF (Fig. 2a, c), we expected that NS3-4A might interfere with the recruitment of TRAF6 by TRIF (Fig. 5a). To examine this possibility, we considered whether or not NS3-4A affects M-pIC-induced NF-κB activation in PH5CH8 cells. Initially, we demonstrated that NF-κB-inducing promoter activity was also enhanced with M-pIC treatment and that this enhancement was mediated by TLR3 and TRIF, as promoter activity was found to be substantially suppressed by TLR3 or TRIF siRNA (Fig. 5b). The results revealed that none of the NS3-4As examined significantly suppressed M-pIC-induced NF-κB activation (Fig. 6a). However, the enhancement of promoter activity in cells expressing CH1-derived NS3-4A was slightly lower than that in cells expressing other strain-derived NS3-4As (Fig. 6a). Therefore, we performed quantitative RT-PCR analysis to examine the levels of IL-6 and IL-8 mRNAs, both of which were induced by NF-κB activation. The results revealed that neither IL-6 nor IL-8 mRNA expression was suppressed in cells expressing CH1-derived NS3-4A (Fig. 6b). These results suggest that TLR3-mediated inflammatory cytokine production was not suppressed by NS3-4A in PH5CH8 cells, and this phenomenon appears to be independent of HCV strain or hepatic disease type.

Fig. 4 None of the NS3-4As derived from patients with different hepatic disease diagnoses prevented M-pIC-induced IFN-β transcription via the TRIF-mediated pathway. **a** Effects of 15 NS3-4As on the activity of the IFN-β gene promoter. PH5CH8 cells transiently expressing NS3-4As from various HCV strains were subjected to M-pIC treatment. PH5CH8 cells transfected with pCX4bsr vector were used as a control (strain, –). The dual luciferase assay was performed as described in Materials and Methods. Data are expressed as the mean ± SD from three independent experiments, each of which was performed in triplicate. **b** Effect of NS3-4As on IFN-β mRNA induction by M-pIC treatment. PH5CH8 cells transiently expressing NS3-4As from several HCV strains containing 1B-5 were subjected to M-pIC treatment. PH5CH8 cells infected with pCX4bsr retrovirus were used as a control (strain, –). Quantitative RT-PCR for IFN-β mRNA was performed in triplicate. The IFN-β mRNA level was calculated relative to the level in control PH5CH8 cells, which was set at 100. **c** None of the NS3-4As cleaved exogenous TRIF. PH5CH8 cells were transfected with myc-TRIF and NS3-4A expression vectors. The production of myc-TRIF and NS3 was analyzed by immunoblot analysis using anti-myc and anti-NS3 antibody, respectively. PH5CH8 cells transfected with the pCX4bsr and pCX4pur vectors were used as a control (–). β-actin was used as a control for the amount of protein loaded per lane. **d** Endogenous TRIF interacts with NS3-4As from various HCV strains but not is cleaved by NS3-4As in PH5CH8 cells. The cell lysates were prepared and subjected to immunoprecipitation using anti-TRIF antibody, followed by immunoblot analysis using anti-TRIF or anti-NS3 antibody, as described in Fig. 2a. Cardif, NS3, and β-actin in the cell lysates were detected by anti-Cardif, anti-NS3, and anti-β-actin antibody, respectively. PH5CH8 cells infected with pCX4bsr retrovirus were used as a control (strain, –)

Discussion

In the present study, we demonstrated that neither IFN-β transcription nor NF-κB activation by extracellular dsRNA was suppressed by NS3-4A, regardless of the source of the HCV strain (e.g., derived from five healthy HCV carriers, a patient with acute hepatitis, seven patients with chronic hepatitis, or two patients with hepatocellular carcinoma). The findings of these studies using PH5CH8 cells suggest that the inhibitory activity of NS3-4A on antiviral signaling pathways is limited to the Cardif-mediated pathway.

Although we confirmed that all of the NS3-4As examined in this study possessed protease activity that enabled the efficient cleavage of the NS5A-NS5B substrate expressed in PH5CH8 cells (data not shown), none of the NS3-4As were able to cleave either exogenous or endogenous TRIF in PH5CH8 cells, although all were able to cleave Cardif. These results suggest that both the non-

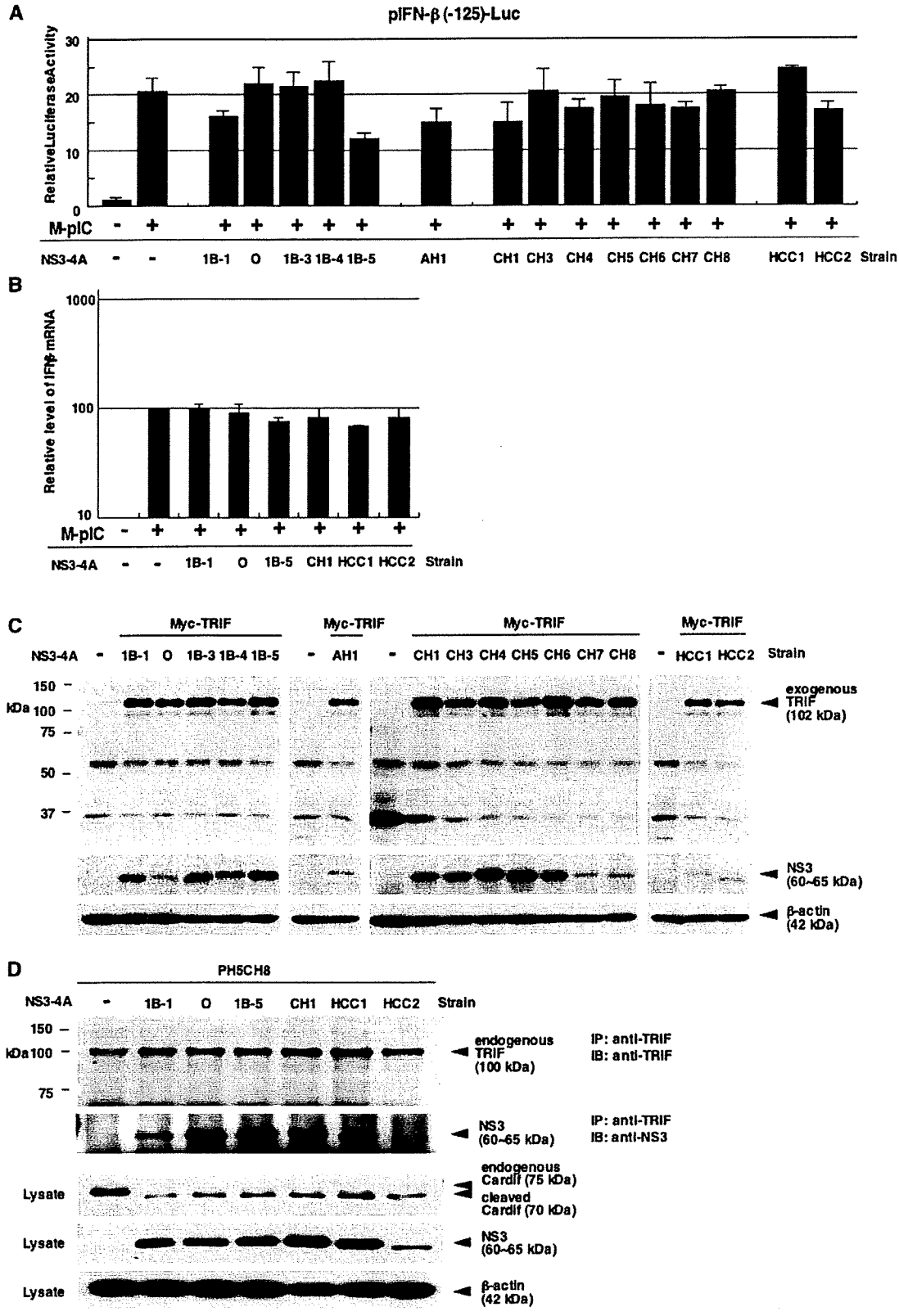
A
pIFN-β(-125)-Luc
RelativeLuciferaseActivity
30
20
10
0
M-pIC - + + + + + + + + + + + + + + + +
NS3-4A - - 1B-1 O 1B-3 1B-4 1B-5 AH1 CH1 CH3 CH4 CH5 CH6 CH7 CH8 HCC1 HCC2 Strain
B
Relative level of IFN-β mRNA
1000
100
10
M-pIC - + + + + + + +
NS3-4A - - 1B-1 O 1B-5 CH1 HCC1 HCC2 Strain
C
Myc-TRIF
Myc-TRIF
Myc-TRIF
Myc-TRIF
NS3-4A - 1B-1 O 1B-3 1B-4 1B-5 - AH1 - CH1 CH3 CH4 CH5 CH6 CH7 CH8 - HCC1 HCC2 Strain
kDa 150 100 75 50 37
exogenous TRIF (102 kDa)
NS3 (60~65 kDa)
β-actin (42 kDa)
D
PH5CH8
NS3-4A - 1B-1 O 1B-5 CH1 HCC1 HCC2 Strain
kDa 150 100 75
endogenous TRIF (100 kDa)
IP: anti-TRIF
IB: anti-TRIF
NS3 (60~65 kDa)
IP: anti-TRIF
IB: anti-NS3
Lysate
endogenous Cardif (75 kDa)
cleaved Cardif (70 kDa)
Lysate
NS3 (60~65 kDa)
Lysate
β-actin (42 kDa)

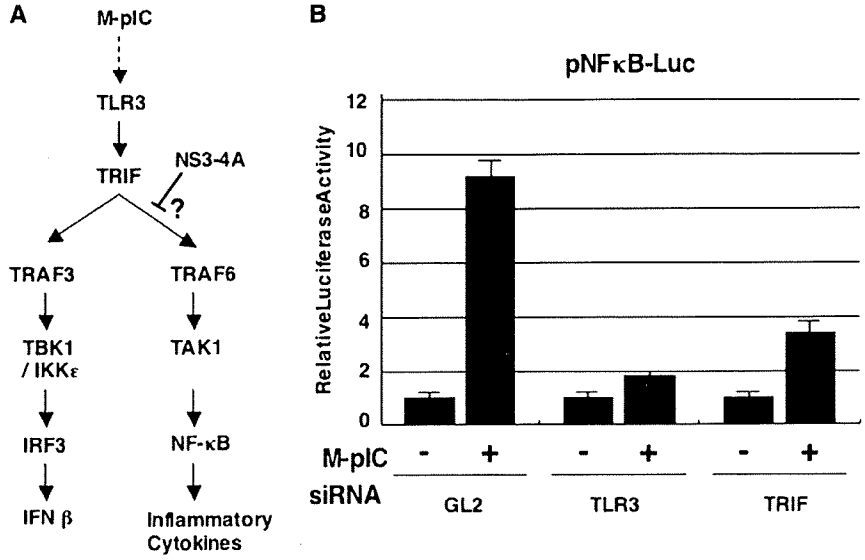

Fig. 5 TLR3-mediated activation of IRF-3 and NF-κB bifurcate at TRIF. **a** Model of TLR3-mediated signaling pathways. **b** Dual luciferase reporter assay of the NF-κB-inducing promoter using siRNA-transfected PH5CH8 cells treated with M-pIC

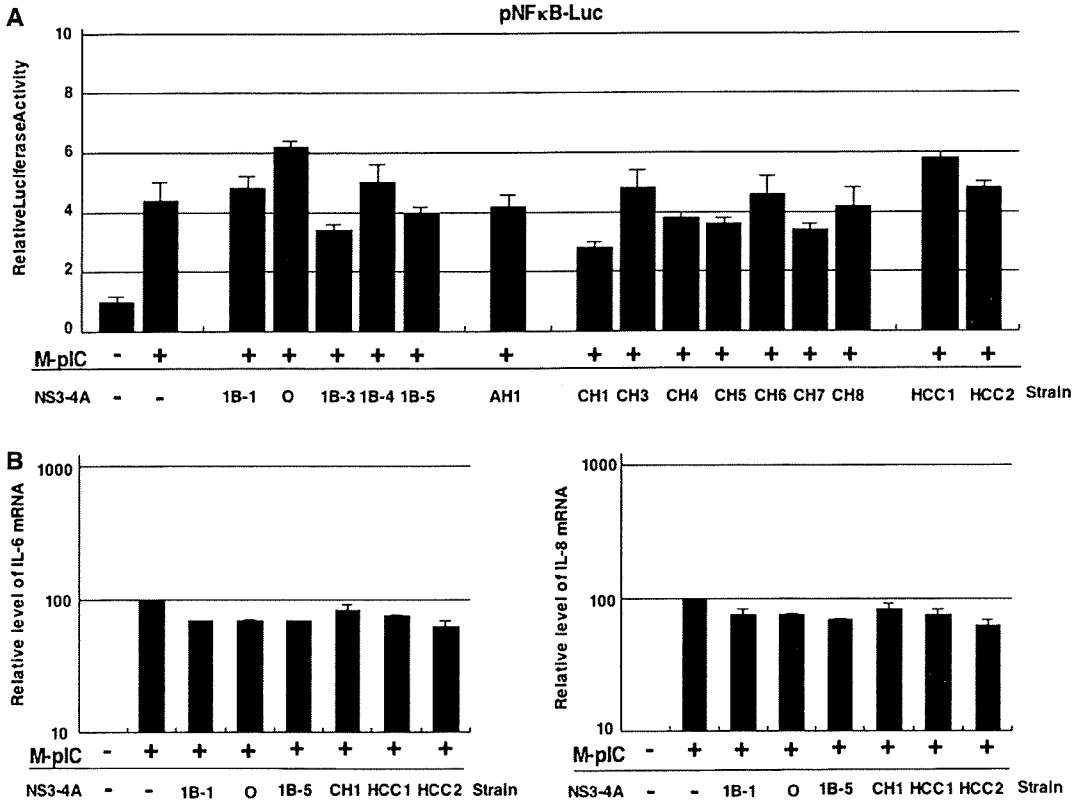

Fig. 6 None of the NS3-4As derived from patients with different hepatic disease diagnoses prevented M-pIC-induced NF-κB activation. **a** Effect of 15 NS3-4As on the activity of NF-κB-inducing promoter. PH5CH8 cells transiently expressing NS3-4As from various HCV strains were subjected to M-pIC treatment. PH5CH8 cells transfected with pCX4bsr vector were used as a control (strain, –). Data are expressed as the mean ± SD from three independent experiments, each of which was performed in triplicate. **b** Effect of NS3-4As on IL-6 or IL-8 mRNA induction by M-pIC treatment. PH5CH8 cells transiently expressing NS3-4A from several strains containing CH1 were subjected to M-pIC treatment. PH5CH8 cells infected with pCX4bsr retrovirus were used as a control (strain, –). Quantitative RT-PCR for IL-6 or IL8 mRNA was performed as described in Fig. 4b

cleavage of TRIF and the cleavage of Cardif by NS3-4A remain unaffected by the genetic diversity observed in NS3-4As derived from 15 different HCV strains (genotype 1b) derived from patients with different stages of hepatic disease as well as different genotypes (1b and 2a). However, other group [10, 27] previously reported that NS3-4A (N strain of genotype 1b) was able to inhibit IFN-β production via the cleavage of TRIF. Although we also observed the interaction of NS3 and TRIF in PH5CH8 and O cells as well as JFH-1-infected RSc cells, the reasons for conflicting results regarding the cleavage of TRIF by NS3-4A are still unclear. To clarify why TRIF is not cleaved by NS3-4A, further analysis will be necessary.

On the other hand, there appear to be some conflicting effects of different HCV proteins on IFN production, as we previously found that the NS5B protein induced IFN-β production in PH5CH8 cells [9, 31] and that the combination of NS5B with the core protein synergistically enhanced IFN-β production [9]. In that study, we showed that enhanced IFN-β production depended on the RNA-dependent RNA polymerase activity of NS5B and on aas 12 and 13 of the core protein, and we observed that NS3-4A significantly inhibited IFN-β production through a combination of the core and NS5B proteins [9]. However, in that case as well, IFN-β production was not completely suppressed by NS3-4A. This may be because NS3-4A is unable to suppress dsRNA-induced and TRIF-mediated IFN-β production, although Cardif-mediated IFN-β production has been shown to be completely suppressed under the same experimental conditions. To clarify the mechanisms underlying the conflicting effects of HCV proteins on IFN-β production mechanisms, an HCV proliferation system using PH5CH8 cells is still needed. However, a HuH-7-cell-based HCV proliferation system [42] would be unsuitable for such purposes due to the functional loss of TLR3 and/or the RIG-I signaling pathway(s) [26, 35]. Studies employing a cell system for HCV proliferation possessing functional TLR3 and/or RIG-I signaling pathways could enhance our understanding of the mechanisms of persistent HCV infection.

Acknowledgments We would like to thank T. Maeta, K. Takemoto, and T. Nakamura for their technical assistance. K. Naka and S. Ohkoshi are also thanked for their valuable input in this study. This work was supported by Grants-in-Aid for the Third-Term Comprehensive Ten-Year Strategy for Cancer Control, and by a Grant-in-Aid for Research on Hepatitis, both from the Ministry of Health, Labor, and Welfare of Japan.

References

1. Akagi T, Sasai K, Hanafusa H (2003) Refractory nature of normal human diploid fibroblasts with respect to oncogene-mediated transformation. Proc Natl Acad Sci USA 100:13567–13572
2. Alam SS, Nakamura T, Naganuma A, Nozaki A, Nouso K, Shimomura H, Kato N (2002) Hepatitis C virus quasispecies in cancerous and noncancerous hepatic lesions: the core protein-encoding region. Acta Med Okayama 56:141–147
3. Alexopoulou L, Holt AC, Medzhitov R, Flavell RA (2001) Recognition of double-stranded RNA and activation of NF-kappaB by Toll-like receptor 3. Nature 413:732–738
4. Benech P, Vigneron M, Peretz D, Revel M, Chebath J (1987) Interferon-responsive regulatory elements in the promoter of the human 2′, 5′-oligo(A) synthetase gene. Mol Cell Biol 7:4498–4504
5. Choo QL, Kuo G, Weiner AJ, Overby LR, Bradley DW, Houghton M (1989) Isolation of a cDNA clone derived from a blood-borne non-A, non-B viral hepatitis genome. Science 244:359–362
6. Dansako H, Ikeda M, Kato N (2007) Limited suppression of the interferon-β production by hepatitis C virus serine protease in cultured human hepatocytes. FEBS J 274:4161–4176
7. Dansako H, Ikeda M, Abe K, Mori K, Takemoto K, Ariumi Y, Kato N (2008) A new living cell-based assay system for monitoring genome-length hepatitis C virus RNA replication. Virus Res 137:72–79
8. Dansako H, Naganuma A, Nakamura T, Ikeda F, Nozaki A, Kato N (2003) Differential activation of interferon-inducible genes by hepatitis C virus core protein mediated by the interferon stimulated response element. Virus Res 97:17–30
9. Dansako H, Naka K, Ikeda M, Kato N (2005) Hepatitis C virus proteins exhibit conflicting effects on the interferon system in human hepatocyte cells. Biochem Biophys Res Commun 336:458–468
10. Ferreon JC, Ferreon AC, Lemon SM (2005) Molecular determinants of TRIF proteolysis mediated by the hepatitis C virus NS3/4A protease. J Biol Chem 280:20483–20492
11. Hijikata M, Kato N, Ootsuyama Y, Nakagawa M, Shimotohno K (1991) Gene mapping of the putative structural region of the hepatitis C virus genome by in vitro processing analysis. Proc Natl Acad Sci USA 88:5547–5551
12. Hijikata M, Mizushima H, Tanji Y, Komada Y, Hirowatari Y, Akagi T, Kato N, Kimura K, Shimotohno K (1993) Proteolytic processing and membrane association of putative nonstructural proteins of hepatitis C virus. Proc Natl Acad Sci USA 90:10773–10777
13. Honda K, Taniguchi T (2006) IRFs: master regulators of signaling by Toll-like receptors and cytosolic pattern-recognition receptors. Nat Rev Immunol 6:644–658
14. Ikeda M, Abe K, Dansako H, Nakamura T, Naka K, Kato N (2005) Efficient replication of a full-length hepatitis C virus genome, strain O, in cell culture, and development of a luciferase reporter system. Biochem Biophys Res Commun 329:1350–1359
15. Ikeda M, Kato N, Mizutani T, Sugiyama K, Tanaka K, Shimotohno K (1997) Analysis of the cell tropism of HCV by using in vitro HCV-infected human lymphocytes and hepatocytes. J Hepatol 27:445–454
16. Ikeda M, Sugiyama K, Mizutani T, Tanaka T, Tanaka K, Sekihara H, Shimotohno K, Kato N (1998) Human hepatocyte clonal cell lines that support persistent replication of hepatitis C virus. Virus Res 56:157–167
17. Jiang Z, Mak TW, Sen G, Li X (2004) Toll-like receptor 3-mediated activation of NF-κB and IRF3 diverges at Toll-IL-1 receptor domain-containing adapter inducing IFN-β. Proc Natl Acad Sci USA 101:3533–3538
18. Kang DC, Gopalkrishnan RV, Wu Q, Jankowsky E, Pyle AM, Fisher PB (2002) mda-5: an interferon-inducible putative RNA helicase with double-stranded RNA-dependent ATPase activity and melanoma growth-suppressive properties. Proc Natl Acad Sci USA 99:637–642

19. Kato N (2001) Molecular virology of hepatitis C virus. Acta Med Okayama 55:133–159
20. Kato N, Hijikata M, Ootsuyama Y, Nakagawa M, Ohkoshi S, Sugiyama T, Shimotohno K (1990) Molecular cloning of the human hepatitis C virus genome from Japanese patients with non-A, non-B hepatitis. Proc Natl Acad Sci USA 87:9524–9528
21. Kato N, Sekiya H, Ootsuyama Y, Nakazawa T, Hijikata M, Ohkoshi S, Shimotohno K (1993) Humoral immune response to hypervariable region 1 of the putative envelope glycoprotein (gp70) of hepatitis C virus. J Virol 67:3923–3930
22. Kishine H, Sugiyama K, Hijikata M, Kato N, Takahashi H, Noshi T, Nio Y, Hosaka M, Miyanari Y, Shimotohno K (2002) Subgenomic replicon derived from a cell line infected with the hepatitis C virus. Biochem Biophys Res Commun 293:993–999
23. Komoda Y, Hijikata M, Sato S, Asabe SI, Kimura K, Shimotohno K (1994) Substrate requirements of hepatitis C virus serine proteinase for intermolecular polypeptide cleavage in *Escherichia coli*. J Virol 68:7351–7357
24. Kuo G, Choo QL, Alter HJ, Gitnick GL, Redeker AG, Purcell RH, Miyamura T, Dienstag JL, Alter MJ, Stevens CE, Tegtmeier GE, Bonino F, Colombo WS, Lee WS, Kuo C, Berger K, Shuster JR, Overby LR, Bradley DW, Houghton M (1989) An assay for circulating antibodies to a major etiologic virus of human non-A, non-B hepatitis. Science 244:362–364
25. Kuroki M, Ariumi Y, Ikeda M, Dansako H, Wakita T, Kato N (2009) Arsenic trioxide inhibits hepatitis C virus RNA replication through modulation of the glutathione redox system and oxidative stress. J Virol 83:2338–2348
26. Lanford RE, Guerra B, Lee H, Averett DR, Pfeiffer B, Chavez D, Notvall L, Bigger C (2003) Antiviral effect and virus-host interactions in response to alpha interferon, gamma interferon, poly(I)-poly(C), tumor necrosis factor alpha, and ribavirin in hepatitis C virus subgenomic replicons. J Virol 77:1092–1104
27. Li K, Foy E, Ferreon JC, Nakamura M, Ferreon AC, Ikeda M, Ray SC, Gale M Jr, Lemon SM (2005) Immune evasion by hepatitis C virus NS3/4A protease-mediated cleavage of the Toll-like receptor 3 adaptor protein TRIF. Proc Natl Acad Sci USA 102:2992–2997
28. Li K, Chen Z, Kato N, Gale M Jr, Lemon SM (2005) Distinct poly(I-C) and virus-activated signaling pathways leading to interferon-beta production in hepatocytes. J Biol Chem 280:16739–16747
29. Li XD, Sun L, Seth RB, Pineda G, Chen ZJ (2005) Hepatitis C virus protease NS3/4A cleaves mitochondrial antiviral signaling protein off the mitochondria to evade innate immunity. Proc Natl Acad Sci USA 102:17717–17722
30. Meylan E, Curran J, Hofman K, Moradpour D, Binder M, Bartenschlager R, Tschopp J (2005) Cardif is an adaptor protein in the RIG-I antiviral pathway and is targeted by hepatitis C virus. Nature 437:1167–1172
31. Naka K, Dansako H, Kobayashi N, Ikeda M, Kato N (2005) Hepatitis C virus NS5B delays cell cycle progression by inducing interferon-beta via Toll-like receptor 3 signaling pathway without replicating viral genomes. Virology 346:348–362
32. Ohkoshi S, Kojima H, Tawaraya H, Miyajima T, Kamimura T, Asakura H, Satoh A, Hirose S, Hijikata M, Kato N, Shimotohno K (1990) Prevalence of antibody against non-A, non-B hepatitis virus in Japanese patients with hepatocellular carcinoma. Jpn J Cancer Res 81:550–553
33. Saito I, Miyamura T, Ohbayashi A, Harada H, Katayama T, Kikuchi Y, Watanabe S, Koi S, Onji M, Ohta Y, Choo QL, Houghton M, Kuo G (1990) Hepatitis C virus infection is associated with the development of hepatocellular carcinoma. Proc Natl Acad Sci USA 87:6547–6549
34. Sato S, Sugiyama M, Yamamoto M, Watanabe Y, Kawai T, Takeda K, Akira S (2003) Toll/IL-1 receptor domain-containing adaptor inducing IFN-beta (TRIF) associates with TNF receptor-associated factor 6 and TANK-binding kinase 1, and activates two distinct transcription factors, NF-kappa B and IFN-regulatory factor-3, in the Toll-like receptor signaling. J Immunol 171:4304–4310
35. RJr Sumpter, Loo YM, Foy E, Li K, Yoneyama M, Fujita T, Lemon SM, MJr Gale (2005) Regulating intracellular antiviral defense and permissiveness to hepatitis C virus RNA replication through a cellular RNA helicase, RIG-I. J Virol 79:2689–2699
36. Tanaka T, Kato N, Cho MJ, Shimotohno K (1995) A novel sequence found at the 3′ terminus of hepatitis C virus genome. Biochem Biophys Res Commun 215:744–749
37. Thomas DL (2000) Hepatitis C epidemiology. Curr Top Microbiol Immunol 242:25–41
38. Ueta M, Hamuro J, Kiyono H, Kinoshita S (2005) Triggering of TLR3 by polyI:C in human corneal epithelial cells to induce inflammatory cytokines. Biochem Biophys Res Commun 331:285–294
39. Xu LG, Wang YY, Han KJ, Li LY, Zhai Z, Shu HB (2005) VISA is an adapter protein required for virus-triggered IFN-β signaling. Mol Cell 19:727–740
40. Yoneyama M, Kikuchi M, Natsukawa T, Shinobu N, Imaizumi T, Miyagishi M, Taira K, Akira S, Fujita T (2004) The RNA helicase RIG-I has an essential function in double-stranded RNA-induced innate antiviral responses. Nat Immunol 5:730–737
41. Yoneyama M, Kikuchi M, Matsumoto K, Imaizumi T, Miyagishi M, Taira K, Foy E, Loo YM, MJr Gale, Akira S, Yonehara S, Kato A, Fujita T (2005) Shared and unique functions of the DExD/H-box helicases RIG-I, MDA5, and LGP2 in antiviral innate immunity. J Immunol 175:2851–2858
42. Wakita T, Pietschmann TT, Kato T, Date T, Miyamoto M, Zhao Z, Murthy K, Habermann A, Krausslich HG, Mizokami M, Bartenschlager R, Liang TJ (2005) Production of infectious hepatitis C virus in tissue culture from a cloned viral genome. Nat Med 11:791–796

Arch Virol (2009) 154:765–773
DOI 10.1007/s00705-009-0366-0

ORIGINAL ARTICLE

Modification of hepatitis C virus 1b RNA polymerase to make a highly active JFH1-type polymerase by mutation of the thumb domain

Leiyun Weng · Jiamu Du · Jingling Zhou · Jianping Ding · Takaji Wakita · Michinori Kohara · Tetsuya Toyoda

Received: 18 December 2008 / Accepted: 16 March 2009 / Published online: 2 April 2009

Abstract Hepatitis C virus (HCV) JFH1 efficiently replicates and produces infectious virus particles in cultured cells. We compared polymerase activity between JFH1 and 1b strains in vitro. The RNA polymerase activity of 1b was 6.4% of that of JFH1. In order to study the mechanism and identify domains responsible for the high polymerase activity of JFH1, we converted the amino acids of 1b RdRp to those of JFH1, and compared their *Km*, *Vmax* and template binding activity. Four amino acid mutations in the thumb domain of 1b RdRp, S377R, A450S, E455N and Y561F increased 1b polymerase activity, and their activity was 23.1, 45.8, 28.9, and 36.1% of JFH1, respectively. *Vmax* and RNA binding activity of JFH1, 1bwt and 1bA450S was JFH1 > 1bA450S > 1b, which indicated both high processivity and slightly higher template binding activity contributed to the high polymerase activity of JFH1.

Electronic supplementary material The online version of this article (doi:10.1007/s00705-009-0366-0) contains supplementary material, which is available to authorized users.

L. Weng · J. Zhou · T. Toyoda (✉)
Unit of Viral Genome Regulation, Institut Pasteur of Shanghai, Chinese Academy of Sciences, 225 South Chongqing Road, 200025 Shanghai, People's Republic of China
e-mail: ttoyoda@sibs.ac.cn

J. Du · J. Ding
State Key Laboratory of Molecular Biology, Institute of Biochemistry and Cell Biology, Shanghai Institutes for Biological Sciences, Chinese Academy of Sciences, 320 Yue-Yang Road, 200031 Shanghai, China

T. Wakita
Department of Virology II, National Institute of Health, 1-23-1 Toyama, Shinjuku, Tokyo 132-8640, Japan

M. Kohara
Department of Microbiology and Cell Biology, Tokyo Metropolitan Institute of Medical Biology, 3-18-22 Honkomagome, Bunkyo-Ku, Tokyo 113-8613, Japan

Abbreviations

HCV	Hepatitis C virus
RdRp	RNA-dependent RNA polymerase
IRES	Internal ribosome entry site
UTR	Untranslated region

Introduction

Hepatitis C virus (HCV) has a positive-stranded RNA genome and belongs to the family *Flaviviridae* [12]. The HCV RNA genome is about 9.6 kb and has a long open reading frame encoding a polyprotein of approximately 3,010 amino acids, which is processed into at least ten viral proteins (NH_2-C-E1-E2-p7-NS2-NS3-NS4A-NS4B-NS5A-NS5B-COOH) by host and viral proteases [6, 7]. The 5′-untranslated region (UTR) contains the internal ribosome entry site (IRES) [21]. The 3′-UTR contains a polypyrimidine "U/C" tract, a variable region, and 98-base X-region [19]. The second stem-loop of the X-region interacts with the NS5BSL3 *cis*-acting replication element (cre) [23].

The soluble NS5B without its C-terminal hydrophobic 21-amino-acid sequence shows RdRp activity in vitro [5, 11]. HCV RdRp exhibits de novo and copy-back (primer-dependent) initiation activities [2, 11, 15, 25]. It can utilize single-stranded RNA as a template but not double-stranded RNA [8, 24]. It favors a cytidine at the 3' terminus of the template, and de novo initiation in vitro by HCV RdRp can be selectively activated by a high GTP concentration [8, 9,

11, 14]. The complementary sequence of IRES shows strong template activity [2, 10, 18]. Structural analysis of HCV 1b RdRp indicates a "closed hand structure" through interaction between the thumb and finger domains with a prominent template channel and suggests that HCV RdRp may change its structure during the initiation of RNA synthesis [4].

Murayama et al. demonstrated that the JFH1 replicon had a more than 1,000 times higher replicon activity than that of J6CF and that the NS3 helicase and NS5B-X-region of JFH1, a strain that replicates efficiently and produces infectious virus particles in Huh7-series cell lines, conferred replication activity on J6CF in Huh7-series cell lines [16]. Their findings also led them to predict that the structural and biochemical differences in RdRp resulted in the difference in replication activity between JFH1 and other HCV strains. In this paper, we have compared the biochemical features of JFH1 RdRp with 1b RdRp and determined the important structural and biochemical features for the strong polymerase activity of JFH1.

Materials and methods

Construction of plasmids expressing HCV RdRp

HCV 1b and JFH1 RdRp without the hydrophobic C-terminal 21 amino acids were PCR-amplified from pVLHCVRdRpwt [11] and pJFH1 [22] and cloned into the *Nhe*I and *Xho*I sites of pET21b (Novagen), resulting in pET21bHCV1bRRdRpΔC21wt and pET21bJFH1RdRpΔC21wt, respectively (Supplementary Table 1). The *Xba*I and *Xho*I fragments of pET21bHCV1bRRdRpΔC21wt and pET21bJFH1RdRpΔC21wt were moved into pET28a (Novagen), resulting in pET28bHCV1bRdRpΔC21wt and pET28bJFH1RdRpΔC21wt, respectively.

Construction of pGEX-HSP90α

cDNA of HSP90α was made by RT-PCR using RNA from 293T cells and cloned into the *Bam*HI and *Xho*I sites of pGEX-6P-3 (GE), resulting in pGEXHSP90α (Supplementary Table 1).

Expression and purification of HCV RdRpΔC21

E. coli Rosetta/pLysS (Novagen) was transformed with pET21bJFH1RdRpΔC21wt and its mutants. Expression of C-terminally 6× His-tagged HCVJFH1RdRpwt and HCVJFH1RdRpD318A was induced with 1 mM IPTG at 18°C for 4 h. *E. coli* Rosetta/pLysS containing pGEX-HSP90α [20] was transformed with pET28bHCV1bRdRΔC21wt. HCV1bRdRpwt expression was induced with 1 mM IPTG at 37°C for 1 h. Then, the cells were suspended in a buffer containing 50 mM NaH_2PO_4 (pH 8.0), 500 mM NaCl, 0.1% Triton X-100, 0.1% 2-mercaptoethanol, 1 mM PMSF, and 2 mM imidazole and lysed by sonication. After centrifugation at 11,000 rpm for 30 min at 4°C (Beckman JA rotor), the supernatant was incubated with Ni-NTA agarose (Qiagen), and the bound JFH1RdRpwt and JFH1RdRpD318A were eluted with elution buffer (500 mM NaCl, 20 mM Tris/HCl, pH 8.0, 0.1% Triton X-100, and 0.1% 2-mercaptoethanol) containing 10 mM imidazole, and 1bRdRpΔC21wt was eluted with buffer containing 250 mM imidazole after the column was washed with 5 mM imidazole. The eluted RdRp was diluted with four volumes of 20 mM HEPES/NaOH, pH 7.5, 1 mM DTT, 1 mM EDTA, and 1 mM PMSF and applied to MonoS in AKTA FPLC (GE) and eluted using a linear gradient from 200 to 1,000 mM NaCl in 20 mM HEPES/NaOH, pH 7.5, 1 mM DTT, 1 mM EDTA, 10% glycerol, and 1 mM PMSF. HCV RdRp was eluted between 520 and 570 mM NaCl.

Table 1 Kinetic constants for HCV RdRp de novo initiation

Nucleotide	JFH1 RdRp	1b A450S RdRp	1bwt RdRp
Km (μM)			
ATP	4.69 ± 0.24	3.90 ± 0.1	3.63 ± 0.21
Low-affinity GTP	87.01 ± 7.24	82.67 ± 1.6	54.67 ± 3.67
CTP	1.71 ± 0.31	1.24 ± 0.21	1.64 ± 0.04
UTP	7.48 ± 0.99	3.88 ± 0.42	3.22 ± 0.08
Vmax (fmol/μg/h)			
ATP	2.87 ± 0.15	0.81 ± 0.03	0.34 ± 0.02
GTP	12.48 ± 1.07	4.17 ± 0.37	2.34 ± 0.1
CTP	0.75 ± 0.07	0.66 ± 0.01	0.30 ± 0.01
UTP	3.30 ± 0.19	3.19 ± 0.17	2.87 ± 0.15

The kinetic constants were calculated from the Lineweaver–Burk plot of polymerase activity (Fig. 4)

Model RNA template

The model RNA template, SL12-1S (184 nucleotides), of the SL12-1S sequence [10] was PCR-amplified from pT702R6X-4 (Supplementary Table 1) and cloned into the *Bam*HI and *Sma*I sites of pBluescript KS+, resulting in pSKSL12-1S. SL12-1S was transcribed in vitro from *Sma*I-digested pKSSL12-1S using MegaShortScript (Ambion).

In vitro transcription

In vitro transcription of HCV RdRp and kinetic analysis were performed as indicated previously [10, 11]. The kinetic constant for UTP was measured using 5 μM [α-^{32}P]CTP.

Table 2 Template-binding constant (*Kass*)

RNA polymerase	JFH1	1bwt	1bL47Q	1bL57T	1bS377R	1bA450S	1bE455N	1bY561F
Kass (pmol/pmol RdRp/h)	0.155	0.130	0.132	0.133	0.144	0.145	0.144	0.140

The template-binding constant was calculated from the Lineweaver–Burk plot of RNA–RdRp complex formation (Fig. 5)

Mutation of HCV RdRp

JFH1RdRpD318A, which has a mutation in its GDD motif, and 1bRdRp mutations of L47Q, L57T, T130P, S377R, A421V, A435V, A450S, E455N, P479H, R517K, and Y561F were introduced using oligonucleotides listed in Supplementary Table 2 with a QuickChange II Site-Directed Mutagenesis Kit (Stratagene). Sequences were confirmed by nucleotide sequencing (Invitrogen).

Filter-binding assay

A model RNA template SL12-1S was transcribed in vitro in 40 mM Tris/HCl, pH 8.0, 8 mM $MgCl_2$, 5 mM DTT, 2 mM spermidine, 0.4 mM of ATP, CTP, GTP, 40 μM UTP, 0.185 Mbq [α-^{32}P] UTP, 1 μg of *Sma*I-digested pKSSL12-1S, and 10 U of T7 RNA polymerase (Takara) at 37°C for 1 hr. After incubation, unincorporated [α-^{32}P] UTP was removed by gel filtration in Quick Spin G-50 columns (Roche), and [^{32}P]-SL12-1S was purified by phenol/chloroform extraction and ethanol precipitation. The filter-binding assay was conducted using the method of Oberste and Flanegan [17]. [^{32}P]SL12-1S (2.5, 5, 10, 25, and 50 pmol) was incubated in 25 μl of 50 mM Tris/HCl, pH 7.5, 200 mM monopotassium glutamate, 3.5 mM $MnCl_2$, 1 mM DTT, and 5 pmol HCV RdRpΔC21 at 29°C for 30 min. After incubation, the solutions were diluted with 0.5 ml TE and filtered through nitrocellulose membranes (0.45 μm, Millipore). The filter was washed five times with TE buffer, and the bound radioisotope was analyzed by Typhoon Trio (GE) after being dried.

Chemicals and radioisotopes

Tris, HEPES, MES, MOPS, imidazole, and actinomycin D were obtained from Sigma, nucleotides were from GE, [α-^{32}P]CTP and [α-^{32}P]UTP were from New England Nuclear, and human placental RNase inhibitor and restriction enzymes were from Takara.

Results

Biochemical analysis of JFH1 and 1b RdRp

1b wild type (1bwt), JFH1 RdRp wild type (JFH1wt) and its GDD-to-GAD mutant (JFH1D318A), which was the knockout mutant of the RNA polymerase domain, were expressed in bacteria and purified by Ni-NTA column chromatography, followed by MonoS ion exchange chromatography (Fig. 1). The biochemical characteristics of 1b and JFH1 RdRp are presented in Fig. 2. Optimal de novo transcription of JFH1 RdRp was obtained in 50 mM Tris/HCl, pH 8.0, 200 mM monopotassium (K) glutamate, 3.5 mM $MnCl_2$, 1 mM DTT, 0.5 mM GTP, 50 μM ATP 50 μM CTP, 5 μM [α-^{32}P]UTP, 0. 2 μM RNA template (SL12-1S), 25 μg/ml actinomycin D, 100 U/ml human placental RNase inhibitor, and 0.1 μM HCV RdRp at 29°C for 90 min after a 30-min preincubation with 0.5 mM GTP. Both RdRps were activated by 0.5 mM GTP preincubation (data not shown). Under optimal conditions, 5 pmol JFH1 RdRp and 1b RdRp transcribed 8.6 ± 1.3 and 0.56 ± 0.12 fmol RNA, respectively. Polymerase activity of 1b RdRp was 6.42 ± 0.43% of JHF1 RdRp (Fig. 3b). JFH1 RdRpD318A had no polymerase activity (data not shown). K-glutamate requirement was measured at 0, 100, 200, 300, 400, 500 and 1,000 mM of K-glutamate in 50 mM Tris/HCl, pH 8.0, 3.5 mM $MnCl_2$ buffer (Fig. 2a). The K-glutamate requirement for 1b RdRp showed a sharp peak at 200 mM, but that for JFH1 RdRp showed a peak at 200 mM with a hump at 300 mM. The Mn^{2+} requirement was measured at 0, 1, 2, 2.5, 3, 3.5, 4, 4.5, 5, 6, 7, 8, 9, and 10 mM $MnCl_2$ in 50 mM Tris/HCl, 200 mM K-glutamate buffer (Fig. 2b). Both RdRp required $MnCl_2$ for polymerase activity. The highest activity of JFH1 RdRp was obtained between 2 and 4 mM $MnCl_2$ with a peak at 3.5 mM, and that of 1b was obtained at 3.5 mM. JFH1 RdRp expressed about 10% activity, with similar dose-dependency, when $MgCl_2$ was used instead of $MnCl_2$. pH sensitivity was measured at pH 4, 5, 6, 6.5, 7, 7.5, 8, 8.5 and 9 (Fig. 2c). The highest activity of JFH1 RdRp was obtained between pH 7.5 and 8.0, but that of 1b RdRp was obtained between pH 6.5 and 7.5. At pH 8.5, 1b RdRp had lost almost all of its activity, while JFH1 retained more than 50%. Polymerase activity was tested at 0, 16, 25, 29, 37 and 42°C (Fig. 2d). The highest activity of JFH1 RdRp was obtained between 25 and 29°C, and that of 1b RdRp was obtained at 29°C. Polymerase activity was not detected with either RdRp at 0 or 42°C.

The kinetic constants (*Km* and *Vmax*) for de novo initiation were measured under optimal transcription conditions with 50, 25, 12.5, 10, 5, 2.5, 2, 1.5, 1, 0.5, 0.25, 0.2, and 0.1 μM of ATP, UTP or CTP, or 500, 400, 300, 200, 100, 50, 25, 12.5, 10, 5, 2.5, 2, 1.5, 1, 0.5, 0.25, 0.2, and

0.1 μM of GTP. *Km* for GTP was measured without pre-incubation. We measured *Km* and *Vmax* for JFH1, 1bwt and 1bA450S RdRp because 1bA450S expressed the highest polymerase activity among the 1b mutants (Fig. 3b). *Km* and *Vmax* are indicated in Table 1, calculated from Lineweaver–Burk plots for HCV JFH1, 1b and 1bA450S RdRp (Fig. 4). The *Km* values for the three RdRps were as follows: *Km* for low-affinity GTP > *Km* for ATP > *Km* for UTP > *Km* for CTP. JFH1 showed a high *Vmax* for GTP (12.48 fmol/μg per h) and ATP (2.87 fmol/μg per h).

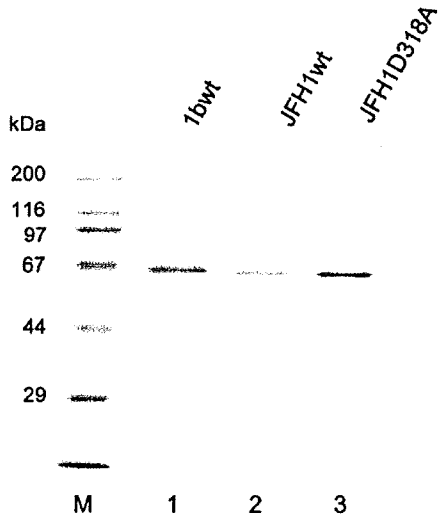

Fig. 1 SDS-PAGE of the purified HCV JFH1 and 1b RNA polymerases. Ten pmol of the purified HCV RdRp was analyzed by 10% SDS-PAGE. The size of molecular standard marker (kDa) is indicated on the left. *M* molecular standard marker (Takara), *1* 1b RdRpwt, *2* JFH1 RdRpwt, *3* JFH1 RdRpD318A

Molecular design of JFH1-type RdRp from 1b RdRp

We focused on the 11 divergent amino acid positions (47, 57, 130, 377, 421, 435, 450, 455, 479, 517 and 561) of JFH1 and 1b RdRp localized on the surface of the molecule (Fig. 6) [3]. The overall level of transcription with the mutant RdRp (5 pmol) was compared to that of JFH1 RdRp (Fig. 3). Among the different amino acid mutations, the polymerase activity of 1bA450S, 1bY561F, 1bE455N, and 1bS377R was 45.8 ± 1.8, 36.1 ± 2.4, 28.9 ± 3.4, and 23.1 ± 1.8% of JFH1, respectively. These all mapped to the thumb domain of 1b RdRp (Fig. 6). However, the polymerase activity of double and triple mutations of 1bA450S (1bS377RA450S, 1bT130PA450S, 1bA450SE455N, 1bS377RA450SP479H, and 1bA450SE455NY561F) was lower than that of 1bA450S. The activity of polymerases with mutations in the

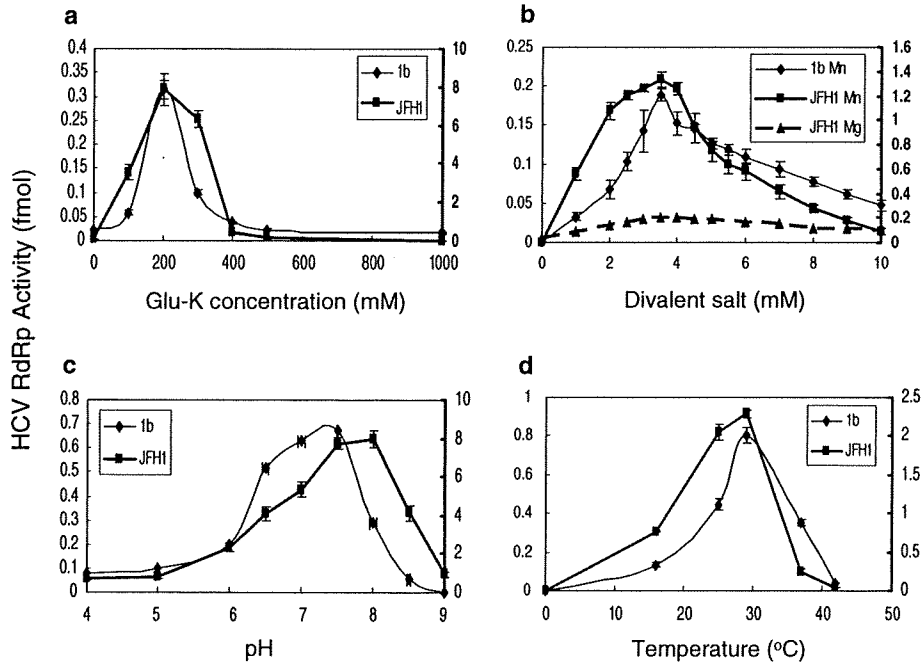

Fig. 2 Biochemical characterization of de novo RNA synthesis by HCV RNA polymerase. The sensitivity of RdRp to monopotassium glutamate (**a**), $MnCl_2$ and $MgCl_2$ (**b**), pH (**c**), and temperature (**d**) were analyzed (see text). For pH sensitivity analysis, 50 mM of MES/NaOH, pH 4.0 and 5.0, MOPS/NaOH, pH 6.0 and 6.5, and 50 mM Tris/HCl, pH 7.0, 7.5, 8.0, 8.5, and 9.0 were used. RdRp activity is presented as the amount of transcribed RNA (fmol). The amount of RNA product (HCV RdRp activity) for 1b RdRp is indicated on the right, and that of JFH1 is indicated on the left. The *symbols* are indicated in each panel. The average and standard deviation of synthesized RNA were calculated from the autoradiograms of three independent experiments

finger domain, 1bL47Q, 1bL57T, and 1bT130P was 15.4 ± 1.4 and 15.3 ± 1.3, and 5.23 ± 0.13%, respectively. The polymerase activity of 1bT130PS377R and 1bR517NY561F was lower than that of 1bS377R and 1bY561F. That of 1bT130PP479H was as low as that of 1bT130P or 1bP479H.

Template-binding activity of HCV RdRp

The template-binding activity of HCV JFH1, 1bwt, and its mutant RdRp, which expressed a higher level of polymerase activity than 1bwt (L47Q, L57T, S377R, A450S, E455N, and Y561F), was examined using [^{32}P]SL12-1S. Five pmol RdRp was incubated with 2.5, 5, 10, 25, and 50 pmol of [^{32}P]SL12-1S. The template-binding constant, *Kass*, is indicated in Table 2, calculated from a Lineweaver–Burk plot of the binding activity obtained from three independent measurements (Fig. 5). The *Kass* of JFH1 RdRp was 0.155 pmol/pmol RdRp/h, the highest value measured, and that of 1b RdRpwt was 0.130 pmol/pmol RdRp/h, the lowest among the RdRps measured so far. Those of 1b RdRp mutants that had higher polymerase activity than the wild type were between 0.155 and 0.130 pmol/pmol RdRp/h.

Discussion

We compared the biochemical and structural features of JFH1 RdRp and 1b RdRp in order to identify the mechanism leading to the high replication activity of the JFH1 strain based on the biochemical characteristics of its RdRp. JFH1 RdRp retains its activity over a wide range of potassium and Mn concentrations and an alkaline pH (Fig. 2).

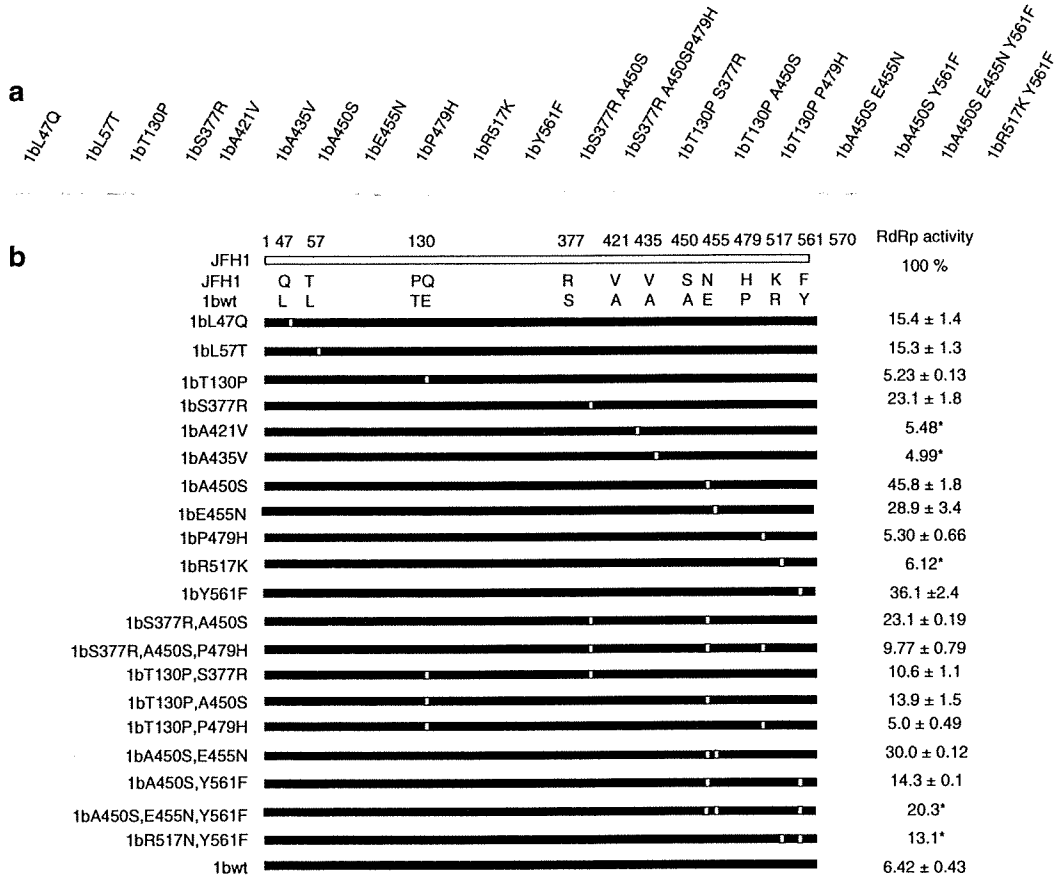

Fig. 3 Polymerase activity of mutant HCV 1b RNA polymerases. **a** The HCV1bRdRp mutants were purified (see "Materials and methods") and 5 pmol of each was applied to 10% SDS-PAGE. **b** The amino acid positions of mutations are indicated by *bars*. RNA polymerase activity of the HCV 1b mutant RdRp were measured, and the activity, with standard deviation, relative to that of JFH1 RdRp was calculated from the autoradiograms of three independent experiments, and this is indicated on the *right side* of the *bars*. *Calculated from one experiment

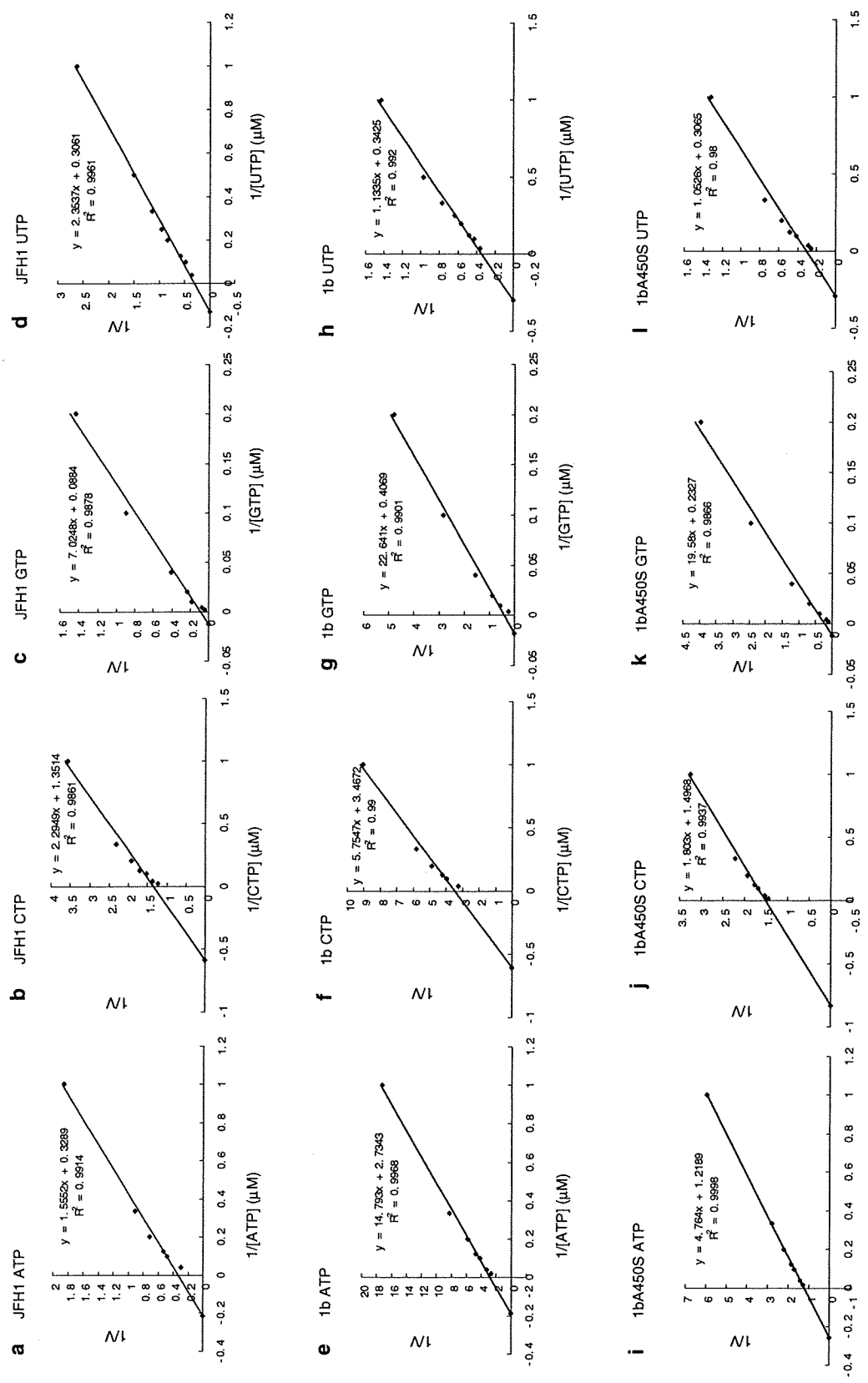

Fig. 4 Lineweaver–Burk plots of HCV JFH1, 1bwt and 1bA450S RNA polymerases. Lineweaver–Burk plots of JFH1 (**a**–**d**), 1bwt (**e**–**h**) and 1bA450S (**i**–**l**) RdRp for ATP (**a**, **e**, **i**), low-affinity GTP (**b**, **f**, **j**), CTP (**c**, **g**, **k**), and UTP (**d**, **h**, **l**) are indicated. The plots were calculated from the average of three independent measurements. The *equation* is indicated in the panel

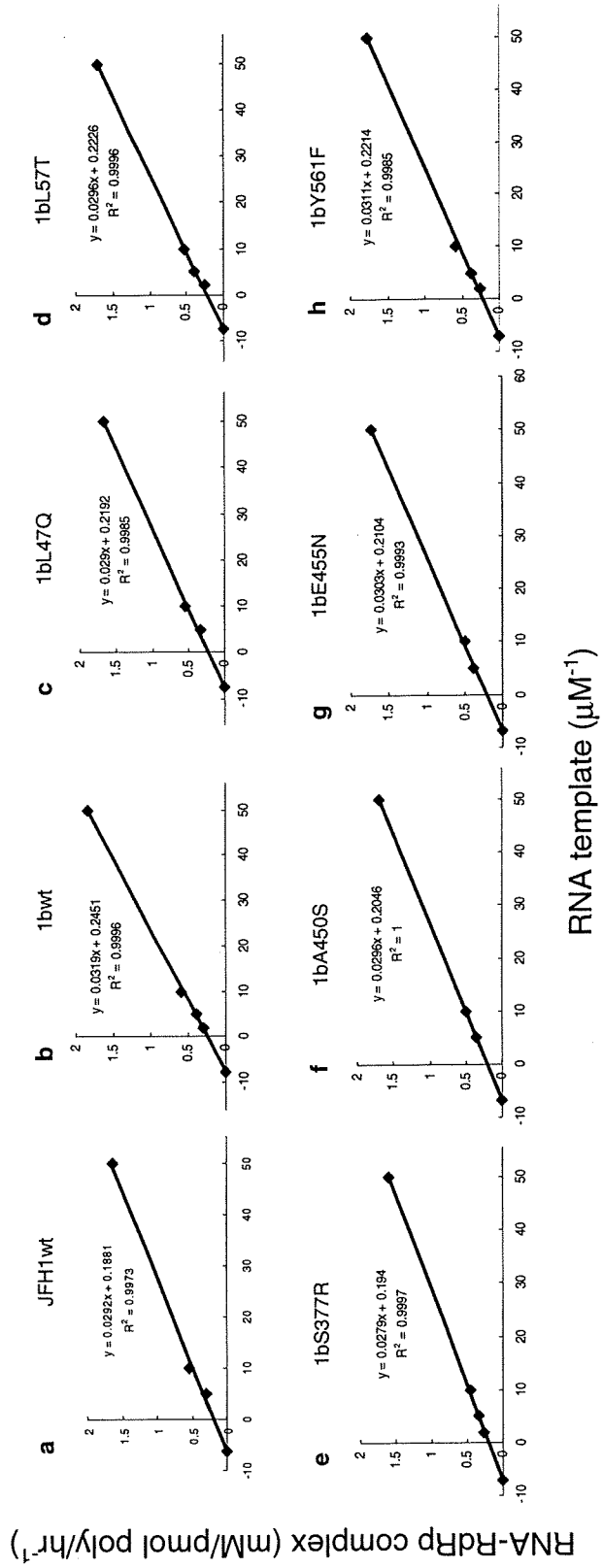

Fig. 5 Template-binding activity of HCV RNA polymerase. Lineweaver–Burk plots of the template-binding activity of HCV IFH1 RdRp (**a**) and 1b RdRpwt (**b**) and 1b mutants. L47Q (**c**), L57T (**d**), S377R (**e**), A450S (**f**), E455N (**g**), and Y561F (**h**) from a filter binding assay using SL12-1S (See "Materials and methods") are shown. The *equation* is indicated in the panel

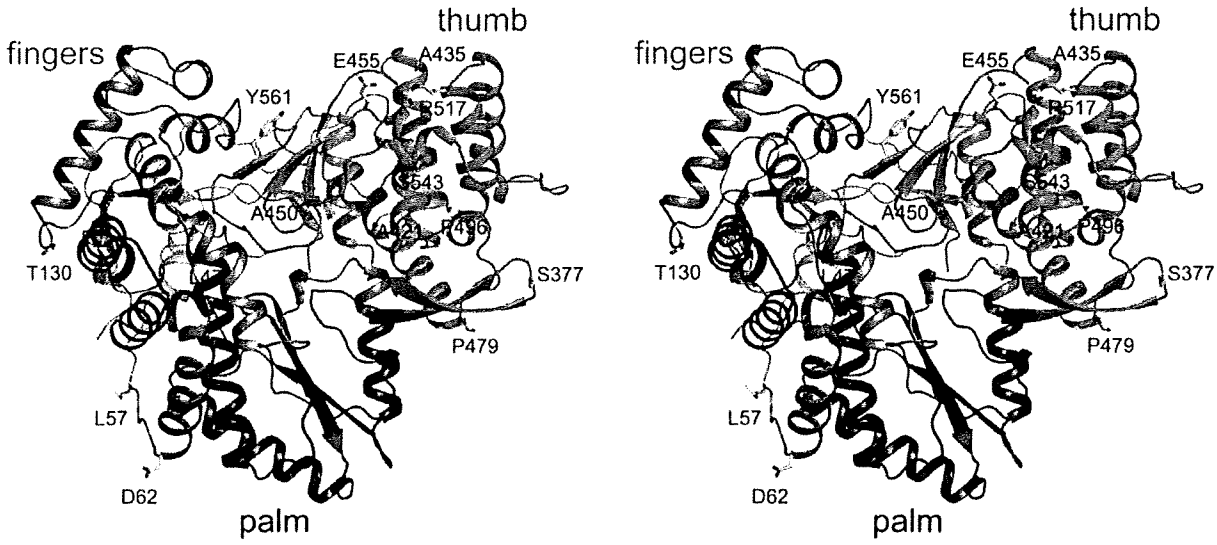

Fig. 6 The positions of the amino acids important for high RdRp activity. A stereogram of HCV 1b RdRp is shown (PDB ID code: 1csj) [3]. The amino acid positions that we mutated are indicated. A450 is located at the *top*, and E455 is located at the *bottom* of the β-finger. Y561 does not interact with the β-finger. The finger domain is indicated in *blue*, the palm in *red*, and the thumb in *green*

JFH1 RdRp showed about 15.4 times higher bulk transcription activity than 1b (Fig. 3). We tried to modify 1b RdRp for the JFH1 type in order to identify the amino acid sequences that are important for the high polymerase activity. The apparent sequence divergence between JFH1 and 1b RdRp is 35 in the ΔC21 molecule (1–570), and we focused on 11 amino acids mapped on the surface of the HCV 1b RdRp molecule: L47Q, L57T, T130P, S377R, A421V, A435V, A450S, E455N, P479H, R517K, and Y561F (Fig. 6). These amino acids are different from those mapped in the template channel [4]. The activity of the mutant 1b RdRp was 1bA450S (46% of JFH1 RdRp) > 1bY561F (36%) > 1bE455N (29%) > 1bS377R (23%). None of the double or triple mutations of these mutants synergistically enhanced the polymerase activity, which indicated that these mutations did not interact with each other (Fig. 3b).

We compared the kinetic constants for de novo initiation of JFH1, 1b and 1bA450S (Table 1). All of the RdRps had *Km* and *Vmax* values similar to those reported previously [11, 15]. HCV RdRp has low affinity for GTP. 1bA450S RdRp had a similar affinity for GTP as JFH1 RdRp. However, its *Vmax* for GTP was not as high as that of JFH1 RdRp. *Vmax* was JFH1 > 1bA450S > 1b, which indicates that efficient polymerizing activity contributes to the high polymerase activity of JFH1 RdRp. However, *Vmax* of JFH1RdRp is not high enough to explain its 15.4-times higher activity than that of 1bRdRpwt. The high *Vmax* of JFH1 with GTP may reflect its efficient initiation using the model template designed for GTP initiation [10].

The template-binding constants (*Kass*) of these mutants ranged between those of 1bwt and of JFH1 (Table 2). The template-binding activity was also JFH1 > 1bA450S > 1bY561F > 1b. All of the mutations enhancing polymerase activity also enhanced the template-binding activity. However, the order of the RNA polymerase activity did not completely fit that of the template-binding activity.

The β-finger of HCV RdRp (443–454) interacts with the C-terminal domain (545–569) and occludes the nucleic-acid-binding pocket of the enzyme [1]. 1b450A is located at the tip and 1b455E is at the bottom of the β-finger, and they may affect the β-finger structure and the space of the template channel formed by the β-finger and thumb domain. 1b561Y does not interact with the β-finger, but 1bY561F may also affect the space of the template channel and template binding. Both the β-finger (450–455) and the β-strand (560–565) play an important role in RNA binding due to their hydrogen-bonding network [13]. The polymerase activity of JFH1S450A was 73.6% of that of JFH1wt. The tip of the β-finger, A450S, and the β-strand of the thumb domain, Y561F, enhanced the 1b RdRp, with a high *Vmax* and RNA-binding activity. Particularly, A450S decreased the affinity of GTP.

In conclusion, both the high *Vmax* and template-binding activity of JFH1 RdRp contribute to its high RdRp activity, although they are not sufficient for this activity. Other factors, including initiation efficiency, remain to be identified.

Acknowledgments This work was supported by grants from Chinese Academy of Sciences (O514P51131 and O812P1A131) and Chinese National Key Project (2008ZX10002-014).

References

1. Ago H, Adachi T, Yoshida A, Yamamoto M, Habuka N, Yatsunami K, Miyano M (1999) Crystal structure of the RNA-dependent RNA polymerase of hepatitis C virus. Structure 7:1417–1426
2. Behrens SE, Tomei L, De Francesco R (1996) Identification and properties of the RNA-dependent RNA polymerase of hepatitis C virus. EMBO J 15:12–22
3. Bressanelli S, Tomei L, Roussel A, Incitti I, Vitale RL, Mathieu M, De Francesco R, Rey FA (1999) Crystal structure of the RNA-dependent RNA polymerase of hepatitis C virus. Proc Natl Acad Sci USA 96:13034–13039
4. Chinnaswamy S, Yarbrough I, Palaninathan S, Ranjith-Kumar CT, Vijayaraghavan V, Demeler B, Lemon SM, Sacchettini JC, Kao CC (2008) A locking mechanism regulates RNA synthesis and host protein interaction by the hepatitis C virus polymerase. J Biol Chem 283:20535–20546
5. Ferrari E, Wright-Minogue J, Fang JW, Baroudy BM, Lau JY, Hong Z (1999) Characterization of soluble hepatitis C virus RNA-dependent RNA polymerase expressed in *Escherichia coli*. J Virol 73:1649–1654
6. Grakoui A, McCourt DW, Wychowski C, Feinstone SM, Rice CM (1993) Characterization of the hepatitis C virus-encoded serine proteinase: determination of proteinase-dependent polyprotein cleavage sites. J Virol 67:2832–2843
7. Hijikata M, Mizushima H, Tanji Y, Komoda Y, Hirowatari Y, Akagi T, Kato N, Kimura K, Shimotohno K (1993) Proteolytic processing and membrane association of putative nonstructural proteins of hepatitis C virus. Proc Natl Acad Sci USA 90:10773–10777
8. Hong Z, Cameron CE, Walker MP, Castro C, Yao N, Lau JY, Zhong W (2001) A novel mechanism to ensure terminal initiation by hepatitis C virus NS5B polymerase. Virology 285:6–11
9. Kao CC, Yang X, Kline A, Wang QM, Barket D, Heinz BA (2000) Template requirements for RNA synthesis by a recombinant hepatitis C virus RNA-dependent RNA polymerase. J Virol 74:11121–11128
10. Kashiwagi T, Hara K, Kohara M, Iwahashi J, Hamada N, Honda-Yoshino H, Toyoda T (2002) Promoter/origin structure of the complementary strand of hepatitis C virus genome. J Biol Chem 277:28700–28705
11. Kashiwagi T, Hara K, Kohara M, Kohara K, Iwahashi J, Hamada N, Yoshino H, Toyoda T (2002) Kinetic analysis of C-terminally truncated RNA-dependent RNA polymerase of hepatitis C virus. Biochem Biophys Res Commun 290:1188–1194
12. Lemon SM, Walker C, Alter MJ, Yi MK (2007) Hepatitis C virus, 5th edn. Lippincott, Philadelphia
13. Leveque VJ, Johnson RB, Parsons S, Ren J, Xie C, Zhang F, Wang QM (2003) Identification of a C-terminal regulatory motif in hepatitis C virus RNA-dependent RNA polymerase: structural and biochemical analysis. J Virol 77:9020–9028
14. Lohmann V, Roos A, Korner F, Koch JO, Bartenschlager R (1998) Biochemical and kinetic analyses of NS5B RNA-dependent RNA polymerase of the hepatitis C virus. Virology 249:108–118
15. Luo G, Hamatake RK, Mathis DM, Racela J, Rigat KL, Lemm J, Colonno RJ (2000) De novo initiation of RNA synthesis by the RNA-dependent RNA polymerase (NS5B) of hepatitis C virus. J Virol 74:851–863
16. Murayama A, Date T, Morikawa K, Akazawa D, Miyamoto M, Kaga M, Ishii K, Suzuki T, Kato T, Mizokami M, Wakita T (2007) The NS3 helicase and NS5B-to-3′X regions are important for efficient hepatitis C virus strain JFH-1 replication in Huh7 cells. J Virol 81:8030–8040
17. Oberste MS, Flanegan JB (1988) Measurement of poliovirus RNA polymerase binding to poliovirion and nonviral RNAs using a filter-binding assay. Nucleic Acids Res 16:10339–10352
18. Reigadas S, Ventura M, Sarih-Cottin L, Castroviejo M, Litvak S, Astier-Gin T (2001) HCV RNA-dependent RNA polymerase replicates in vitro the 3′ terminal region of the minus-strand viral RNA more efficiently than the 3′ terminal region of the plus RNA. Eur J Biochem 268:5857–5867
19. Tanaka T, Kato N, Cho MJ, Sugiyama K, Shimotohno K (1996) Structure of the 3′ terminus of the hepatitis C virus genome. J Virol 70:3307–3312
20. Tolia NH, Joshua-Tor L (2006) Strategies for protein coexpression in *Escherichia coli*. Nat Methods 3:55–64
21. Tsukiyama-Kohara K, Iizuka N, Kohara M, Nomoto A (1992) Internal ribosome entry site within hepatitis C virus RNA. J Virol 66:1476–1483
22. Wakita T, Pietschmann T, Kato T, Date T, Miyamoto M, Zhao Z, Murthy K, Habermann A, Krausslich HG, Mizokami M, Bartenschlager R, Liang TJ (2005) Production of infectious hepatitis C virus in tissue culture from a cloned viral genome. Nat Med 11:791–796
23. You S, Stump DD, Branch AD, Rice CM (2004) A *cis*-acting replication element in the sequence encoding the NS5B RNA-dependent RNA polymerase is required for hepatitis C virus RNA replication. J Virol 78:1352–1366
24. Zhong W, Ferrari E, Lesburg CA, Maag D, Ghosh SK, Cameron CE, Lau JY, Hong Z (2000) Template/primer requirements and single nucleotide incorporation by hepatitis C virus nonstructural protein 5B polymerase. J Virol 74:9134–9143
25. Zhong W, Uss AS, Ferrari E, Lau JY, Hong Z (2000) De novo initiation of RNA synthesis by hepatitis C virus nonstructural protein 5B polymerase. J Virol 74:2017–2022

JOURNAL OF VIROLOGY, May 2009, p. 5137–5147 Vol. 83, No. 10
0022-538X/09/$08.00+0 doi:10.1128/JVI.02179-08

Involvement of Creatine Kinase B in Hepatitis C Virus Genome Replication through Interaction with the Viral NS4A Protein[▽]

Hiromichi Hara,[1,2] Hideki Aizaki,[1] Mami Matsuda,[1] Fumiko Shinkai-Ouchi,[3] Yasushi Inoue,[1,4] Kyoko Murakami,[1] Ikuo Shoji,[1,5] Hayato Kawakami,[6] Yoshiharu Matsuura,[7] Michael M. C. Lai,[8] Tatsuo Miyamura,[1] Takaji Wakita,[1] and Tetsuro Suzuki[1]*

Department of Virology II[1] and Department of Biochemistry and Cell Biology,[3] National Institute of Infectious Diseases, Tokyo 162-8640, Japan; Department of Internal medicine, Division of Pulmonary Diseases, The Jikei University School of Medicine, Tokyo 105-8461, Japan[2]; Mita Hospital, International University of Health and Welfare, Tokyo 108-8329, Japan[4]; Division of Microbiology, Kobe University Graduate School of Medicine, Hyogo 650-0017, Japan[5]; Department of Anatomy, Kyorin University School of Medicine, Tokyo 181-8611, Japan[6]; Research Institute for Microbial Diseases, Osaka University, Osaka 565-0871, Japan[7]; and Department of Molecular Microbiology and Immunology, University of Southern California, Keck School of Medicine, Los Angeles, California 90033[8]

Received 15 October 2008/Accepted 20 February 2009

Persistent infection with hepatitis C virus (HCV) is a major cause of chronic liver diseases. The aim of this study was to identify host cell factor(s) participating in the HCV replication complex (RC) and to clarify the regulatory mechanisms of viral genome replication dependent on the host-derived factor(s) identified. By comparative proteome analysis of RC-rich membrane fractions and subsequent gene silencing mediated by RNA interference, we identified several candidates for RC components involved in HCV replication. We found that one of these candidates, creatine kinase B (CKB), a key ATP-generating enzyme that regulates ATP in subcellular compartments of nonmuscle cells, is important for efficient replication of the HCV genome and propagation of infectious virus. CKB interacts with HCV NS4A protein and forms a complex with NS3-4A, which possesses multiple enzyme activities. CKB upregulates both NS3-4A-mediated unwinding of RNA and DNA in vitro and replicase activity in permeabilized HCV replicating cells. Our results support a model in which recruitment of CKB to the HCV RC compartment, which has high and fluctuating energy demands, through its interaction with NS4A is important for efficient replication of the viral genome. The CKB-NS4A association is a potential target for the development of a new type of antiviral therapeutic strategy.

Hepatitis C virus (HCV) infection represents a significant global healthcare burden, and current estimates suggest that a minimum of 3% of the world's population is chronically infected (4, 19). The virus is responsible for many cases of severe chronic liver diseases, including cirrhosis and hepatocellular carcinoma (4, 16, 19). HCV is a positive-stranded RNA virus belonging to the family *Flaviviridae*. Its ~9.6-kb genome is translated into a single polypeptide of about 3,000 amino acids (aa), in which the nonstructural (NS) proteins NS2, NS3, NS4A, NS4B, NS5A, and NS5B reside in the C-terminal half region (6, 34, 44). NS4A, a small 7-kDa protein, functions as a cofactor for NS3 to enhance NS3 enzyme activities such as serine protease and helicase activities. The hydrophobic N-terminal region of NS4A, which is predicted to form a transmembrane α-helix, is responsible for membrane anchorage of the NS3-4A complex (8, 44, 50), and the central region of NS4A is important for the interaction with NS3 (10, 44). A recent study demonstrated the involvement of the C terminus of NS4A in the regulation of NS5A hyperphosphorylation and viral replication (28).

The development of HCV replicon technology several years ago accelerated research on viral RNA replication (7, 44). Furthermore, a robust cell culture system for propagation of infectious HCV particles was developed using a viral genome of HCV genotype 2a, JFH-1 strain, enabling us to study every process in the viral life cycle (27, 47, 54). RNA derived from genotype 1a, HCV H77, containing cell-culture adaptive mutations, also produces infectious viruses (52). Using these systems, it has been reported that the HCV genome replicates in a distinct, subcellular replication complex (RC) compartment, which includes NS3-5B and the viral RNA (2, 14, 33). The RC forms in a distinct compartment with high concentrations of viral and cellular components located on detergent-resistant membrane (DRM) structures, possibly a lipid-raft structure (2, 41), which may protect the RC from external proteases and nucleases. Almost all processes in viral replication are dependent on the host cell's machinery and involve intimate interaction between viral and host proteins. However, the functional roles of host factors interacting with the HCV RC in viral genome replication remain ambiguous.

To gain a better understanding of cellular factors that are components of the HCV RC and that function as regulators of viral replication, a comparative proteomic analysis of DRM fractions from HCV replicon and parental cells and subsequent RNA interference (RNAi) silencing of selected genes were performed. We identified creatine kinase B (CKB) as a key factor for the HCV genome replication. CKB catalyzes the reversible transfer of the phosphate group of phosphocreatine

* Corresponding author. Mailing address: Department of Virology II, National Institute of Infectious Diseases, 1-23-1 Toyama, Shinjuku-ku, Tokyo 162-8640, Japan. Phone: 81-3-5285-1111. Fax: 81-3-5285-1161. E-mail: tesuzuki@nih.go.jp.

▽ Published ahead of print on 4 March 2009.

(pCr) to ADP to yield ATP and creatine and is known to play important roles in local delivery and cellular compartmentalization of ATP (48, 51). The findings obtained here suggest that recruitment of CKB to the HCV RC, through CKB interaction with NS4A, is essential for maintenance or enhancement of viral replicase activity.

MATERIALS AND METHODS

Cell lines, antibodies, and reagents. Human hepatoma cell line Huh-7.5.1 (54) was kindly provided by Francis V. Chisari. Cell lines carrying subgenomic replicon RNAs, namely, SGR-N (41) and SGR-JFH1 (23), were derived from the HCV-N (17) and JFH-1 strains (24), respectively. Mouse monoclonal antibodies (MAbs) against HCV NS3 (Chemicon, Temecula, CA), NS4A (Santa Cruz Biotechnology, Inc., Santa Cruz, CA), NS5A (Biodesign, Saco, ME), NS5B (2), FLAG (M2; Sigma-Aldrich, St. Louis, MO), glyceraldehyde-3-phosphate dehydrogenase (GAPDH; Chemicon), and Flotillin-1 (BD Biosciences, San Jose, CA) and polyclonal antibodies (PAbs) against CKB (mouse [Abnova, Taipei, Taiwan], goat [Santa Cruz]), hemagglutinin (HA; Sigma-Aldrich), and FLAG (Sigma-Aldrich) were used. Cyclocreatine (Ccr; also known as 2-imino-1-imidazolidineacetic acid), pCr, and phosphopyruvic acid (pPy) were purchased from Sigma-Aldrich. Recombinant CKB and pyruvate kinase (PK) were obtained from Acris (Herfold, Germany) and Calbiochem (San Diego, CA), respectively.

Proteome analysis. RC-rich membrane fractions of cells were isolated as described previously (2, 41). Briefly, cells were lysed in hypotonic buffer. After removing the nuclei, supernatants were treated with 1% NP-40 for 60 min, mixed with 70% sucrose, overlaid with 55 and 10% sucrose, and centrifuged at 38,000 rpm for 14 h. Proteins from membrane fractions were purified by using a 2D Clean-Up kit (GE Healthcare, Tokyo, Japan), followed by labeling with fluorescent dyes: Cy5 for replicon cells, Cy3 for parental cells, and Cy2 for the protein standard containing equal amounts of both cell samples. Two-dimensional fluorescence difference gel electrophoresis (2D-DIGE) was performed using Immobiline DryStrip as the first-dimension gel and 12.5% polyacrylamide gel as the second-dimension gel. The 2D-DIGE images were analyzed quantitatively using the DeCyder software (GE Healthcare). Student *t* test was performed on differences between the tested samples using DeCyder biological variation analysis module. Samples were analyzed in triplicate. The protein spots of interest were excised from the gel, subjected to in-gel digestion using trypsin or lysyl endopeptidase and analyzed by liquid chromatography (MAGIC 2002 System; Michrom Bioresources, Auburn, CA) directly connected to electrospray ionization-ion trap mass spectrometry (LCQ-decaXP; Thermo Electron Corp., Iwakura, Japan). The results were subjected to database (NCBInr) search by Mascot server software (Matrix Science, Boston, MA) for peptide assignment.

Plasmids. A human CKB cDNA (43; kindly provided by Oriental Yeast Corp., Tokyo, Japan) was inserted into the EcoRI site of pCAGGS, yielding pCAGCKB. To generate expression plasmids for HA-tagged versions of wild-type and deletion mutated CKB, the corresponding DNA fragments were amplified by PCR, followed by introduction into the BglII site of pCAGGS. A fragment representing the inactive mutant CKB-C283S was synthesized by PCR mutagenesis. To generate FLAG-tagged NS protein expression plasmids, DNA fragments encoding either NS3, NS4A, NS4B, NS5A, or NS5B protein were amplified from HCV strains NIHJ1 (1) and JFH-1 (23) by PCR, followed by cloning into the EcoRI-EcoRV sites of pcDNA3-MEF (20). To generate an HA-tagged NS3 expression plasmid, a fragment encoding NS3 with the HA tag sequence at its N terminus was inserted into pCAGGS.

siRNA transfection. The small interfering RNAs (siRNAs) targeted to CKB (CKB-1 [5′-UAAGACCUUCCUGGUGUGGTT-3′] and CKB-2 [5′-CGUCAC CCUUGGUAGAGUUTT-3′]) and the scramble negative control siRNA to CKB-2 (5′-GGCGUACUAGCUUAUUCGCTT-3′) were purchased from Sigma. Cells in a 24-well plate were transfected with siRNA using HiPerFect transfection reagent (Qiagen, Tokyo, Japan) according to the manufacturer's instructions. The siRNA sequences for the other genes used in the siRNA screening are available upon request.

HCV infection. Culture media from Huh-7 cells transfected with in vitro-transcribed RNA corresponding to the full-length JFH-1 (47) was collected, concentrated, and used for the infection assay (3).

Quantification of HCV core protein and RNA. To estimate the levels of HCV core protein, aliquots of culture supernatants or of cell lysates were assayed by using HCV Core enzyme-linked immunosorbent assay kits (5). Total RNA was isolated from harvested cells using TRIzol (Invitrogen, Carlsbad, CA). Copy numbers of the viral RNA were determined by reverse transcription-PCR (RT-PCR) (2, 36, 46).

Immunoprecipitation, immunoblot analysis, and immunofluorescence microscopy. The analyses, as well as DNA transfection, were performed essentially as previously described (42). Cells were lysed in immunoprecipitation lysis buffer (50 mM Tris-HCl [pH 7.6], 150 mM NaCl, 1% sodium deoxycholate, 1% NP-40, 0.1% sodium dodecyl sulfate, 1 mM dithiothreitol, 1 mM calcium acetate). For immunoprecipitation, supernatants of cell lysates were precipitated with anti-FLAG antibody and protein A-Sepharose Fast Flow beads (GE healthcare). For immunofluorescence microscopy, anti-CKB goat PAb and anti-NS4A MAb as primary antibodies and Alexa Fluor 555-conjugated donkey anti-goat immunoglobulin G (Invitrogen) and Alexa Fluor 488-conjugated rabbit anti-mouse immunoglobulin G (Invitrogen) as secondary antibodies were used and observed under an LSM 510 confocal microscope (Carl Zeiss, Oberkochen, Germany).

Immunoelectron microscopy. Postembedding immunostaining using the colloidal gold-labeling method was performed as described previously (38). Cells were fixed in 4% paraformaldehyde–1% glutaraldehyde at 4°C for 1 h. After dehydration through a graded series of ethanol, cells were embedded in LR White (London Resin Company, London, United Kingdom) and sectioned. After blocking, section grids were incubated with a mixture of anti-NS4A and anti-CKB antibodies at 4°C overnight, followed by treatment with a mixture of 18-nm colloidal gold-conjugated donkey anti-mouse immunoglobulin G and 12-nm colloidal gold-conjugated donkey anti-goat immunoglobulin G antibodies (Jackson Immunoresearch, West Grove, PA) at 4°C overnight. The sections were stained with uranyl acetate and observed under a transmission electron microscope.

Measurement of CK activity and cellular ATP level. Cells were lysed with passive lysis buffer (Promega, Madison, WI), and CK activities were measured based on Oliver methods (40), in which the activity of converting creatine phosphate and ADP to creatine and ATP was measured. ATP levels in cell lysates were measured by using a CellTiter-Glo luminescent cell viability assay (Promega).

RNA replication assays in permeabilized replicon cells and in vitro. The RNA synthesis assay using permeabilized replicon cells was based on a previously described method (33). Briefly, SGR-JFH1 cells were treated with 5 μg of actinomycin D/ml for 2 h, followed by permeabilization with 50 μg of digitonin/ml for 5 min. The resulting mix was incubated with 500 μM concentrations of ATP, GTP, and CTP; 10 μCi of UTP ([α-^{32}P]UTP); 50 μg of actinomycin D/ml; and 5 mM pCr with or without 20 U of CKB/ml for 4 h at 27°C. RNA was extracted by using TRIzol and analyzed by 1% formaldehyde agarose gel electrophoresis. The cell-free RNA replication assay was performed as described previously (2).

In vitro helicase assays. Helicase activity on double-stranded RNA (dsRNA) was investigated as described previously (11) with some modifications. The 5′ end of the release strand was labeled with [γ-^{32}P]ATP using T4 polynucleotide kinase (Ambion). The dsRNA substrate was obtained by annealing the labeled RNA with a template strand RNA at a molar ratio of 1:1. The helicase assay mixture contained 5 nM dsRNA, helicase enzyme (80 nM NS3 or NS3-4A [kindly provided by R. De Francesco]), 6 mM ATP, in the presence or absence of 20 U of CKB/ml in an assay buffer (25 mM MOPS-NaOH [pH 7.0], 2.5 mM dithiothreitol, 100 μg of bovine serum albumin/ml, 3 mM $MgCl_2$, 5 mM pCr, 2.5 U of RNase inhibitor/ml). After the helicase reaction, samples were electrophoresed in a native 8% polyacrylamide gel and autoradiographed.

To determine the effect of PK/pPy system on the helicase activity, PK and pPy were used instead of CKB and pCr. Helicase activity on dsDNA was measured based on homogeneous time-resolved fluorescence quenching using a Trupoint helicase assay kit (Perkin-Elmer, Waltham, MA) according to the manufacturer's instructions.

In vitro protease assay. In vitro HCV protease activity of NS3-4A or NS3 was analyzed by using a SensoLyteHCV protease assay kit (AnaSpec, San Jose, CA) according to the manufacturer's instructions.

RESULTS

Identification of host factors involved in HCV RNA replication by comparative proteomic analysis of DRM fractions and RNAi silencing. To identify host proteins involved in the HCV RC, proteome profiles of the RC-rich membrane fraction in Huh-7 cells harboring subgenomic replicon RNA derived from genotype 1b, N isolate (SGR-N) were compared to those of parental cells by 2D-DIGE. We confirmed that the DRM fraction obtained from SGR-N cells is functionally active in a

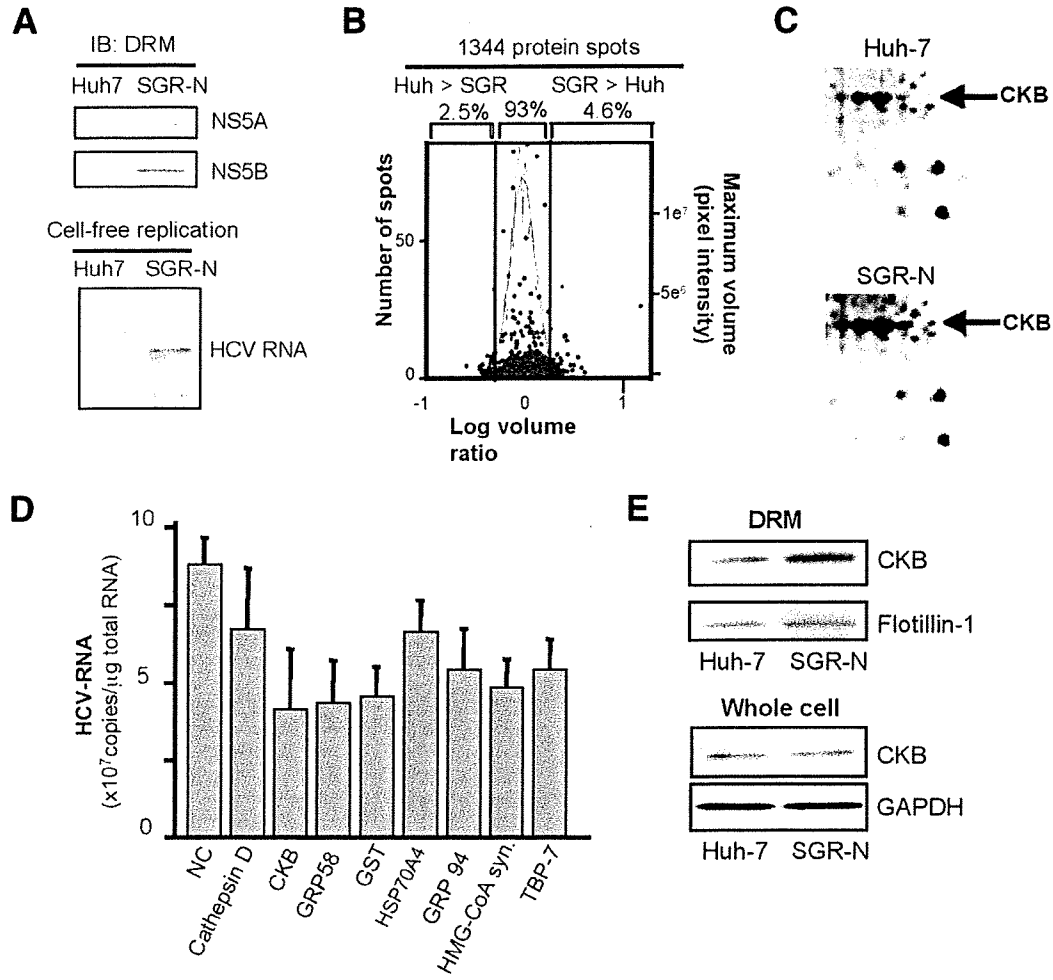

FIG. 1. Comparative proteomic analysis of DRM fractions and RNAi silencing. (A) Preparation of functionally active RC fraction for proteome analysis. DRM fractions obtained from SGR-N cells and parental Huh-7 cells were analyzed by immunoblotting with anti-NS5A and anti-NS5B antibodies (upper panel) and by the cell-free RNA replication assay (lower panel). (B) Histogram representation of proteins detected in 2D-DIGE. Images were analyzed quantitatively by the DeCyder software. The left and right *y* axis, respectively, indicate the spot frequency and the maximum volume of each spot, given against the log volume ratio (*x* axis). (C) Comparison of 2D-DIGE maps of proteins from DRM fractions of SGR-N cells and Huh-7 cells. Enlarged 2D-DIGE gel images of regions containing protein spots of CKB (arrows) are shown. (D) Effects of siRNAs of genes selected from comparative proteome analysis on HCV RNA replication. SGR-N cells were transfected with siRNA specific to cathepsin D, CKB (siCKB-1), GRP58, GST, Hsp70 protein 4, GRP94, HMG-coenzyme A synthase, or Tat binding protein 7 or with nontargeting (NC) siRNA. At 48 h posttransfection, total RNA was isolated and HCV RNA levels were assessed by real-time RT-PCR. (E) Enrichment of CKB in the DRM of HCV replicon cells. Equal amounts of DRM fractions from SGR-N and parental Huh-7 cells, or whole-cell lysates from both cells were analyzed by immunoblotting with antibodies against CKB, flotilin-1 or GAPDH.

cell-free replication assay (Fig. 1A). Three independent proteome experiments were performed for a reliable analysis of protein expression. Approximately 1,300 spots were resolved in each gel, and 4 to 5% of the protein spots represented a >2-fold increase in the membrane fraction of replicon cells in each experiment (Fig. 1B). The protein spots that exhibited high reproducibility (an example shown in Fig. 1C) were excised, digested by trypsin or lysyl endopeptidase, and analyzed by mass spectrometry, which identified the corresponding proteins in 27 cases (Table 1). Among the proteins implicated in a variety of functional categories, 10 were involved in protein folding, mainly as chaperones, 7 were metabolic and biosynthesis enzymes including proteins for redox regulation or energy pathways, 3 were involved in cytoskeleton organization, and 3 proteins were related to cellular processes, mainly proteolysis pathways. The viral NS proteins identified as differentially expressed proteins in the analysis were not listed.

In order to identify host factors involved in HCV replication, we examined the effects on viral RNA replication of transfection of SGR-N cells with siRNAs against genes encoding nine proteins belonging to diverse classes of biological functions (Table 1). Each siRNA reduced the HCV RNA level to 47 to 76% of the level of the siRNA control (Fig. 1D). None of the siRNAs tested exhibited considerable cytotoxicity against the replicon cells, ruling out overt toxicity as a mechanism for inhibition of viral RNA replication. Among the candidate

TABLE 1. Selected proteins that reproducibly increased in the DRM fraction of SGR-N cells[a]

Avg ratio	*P* (Student *t* test)	Coverage (%)	Protein name	Molecular function	GI no.
5.56	0.04	27	GRP94	Protein folding	15010550
4.99	0.07	47	Hsp60	Protein folding	6996447
3.73	0.07	6	tRNA guanine transglycosylase	Metabolism	30583205
3.56	0.06	23	KIAA0088	Unknown	577295
3.32	0.07	4	Thioredoxin-related protein	Unknown	20067392
3.32	0.13	12	Tat binding protein 1 (TBP-1)	Cellular processes	20532406
3.06	0.14	22	Aldehyde dehydrogenase 1	Metabolism	2183299
3.06	0.14	14	Chaperonin TRiC/CCT, subunit 2	Protein folding	54696794
2.96	0.04	14	Heat shock 70-kDa protein 4 (HSPA4)	Protein folding	6226869
2.96	0.04	29	GRP58	Metabolism/protein folding	2245365
2.94	0.01	37	Mutant β-actin	Cytoskeleton organization	28336
2.65	0.17	33	Glutathione S-transferase (GST)	Catalytic activity	2204207
2.53	0.04	37	Keratin 19	Cytoskeleton organization	6729681
2.46	0.08	6	Heterogeneous nuclear ribonucleoprotein K	Nucleic acid modification	460789
2.45	0.001	13	HMG-coenzyme A synthase	Metabolism	30009
2.4	0.02	31	CKB	Energy pathway/metabolism	180570
2.4	0.02	11	Cathepsin D	Cellular processes	30582659
2.4	0.02	11	C8orf2	Unknown	37181322
2.36	0.1	38	Tropomyosin 4-anaplastic lymphoma kinase fusion protein	Cytoskeleton organization	14010354
2.36	0.1	6	Calreticulin	Protein folding	30583735
2.33	0.01	29	Quinolinate phosphoribosyltransferase	Metabolism	30583301
2.29	0.04	25	Protein disulfide isomerase-related protein 5	Protein folding	1710248
2.29	0.04	16	Tat binding protein 7 (TBP-7)	Cellular processes	263099
2.05	0.11	24	Calumenin	Metabolism	2809324
2.05	0.12	10	TRiC/CCT, subunit 5	Protein folding	24307939
2.03	0.07	20	Hsp90 beta	Protein folding	34304590
2.01	0.07	10	TRiC/CCT, subunit 1	Protein folding	36796

[a] The spectra obtained by tandem mass spectrometry were collected using data-dependent mode, and the results were subjected to database (NCBInr) search by Mascot server software (Matrix Science, London, United Kingdom) for peptide assignment. Coverage, the ratio of the portion of protein sequence covered by matched peptides to the whole protein sequence. GI no., GenInfo identifier number.

genes examined, we observed a reproducible inhibition of HCV RNA replication by two independent siRNAs targeting CKB (see below).

CKB participates in HCV RNA replication and the propagation of infectious virus. CKB is a brain-type creatine kinase isoenzyme and is also detected in a variety of other tissues, including human liver (32). Steady-state levels of CKB in the DRM fraction, as well as in whole-cell lysate of SGR-N cells were compared to those from parental cells by Western blotting. The CKB level in the DRM fraction of replicon cells was higher than that in parental cells (Fig. 1E), confirming the results of the proteome analysis described above. In contrast, the CKB level in whole cells was similar in both cells (Fig. 1E). These results suggest participation of posttranslational modification, such as translocation to the DRM fraction, of CKB in replicon cells.

Figure 2A shows the inhibitory effect on HCV RNA replication of CKB siRNA; siCKB-2, the sequence of which does not overlap with the sequence of siCKB-1 used in the above siRNA screening (Fig. 1D). Transfection with siCKB-2 effectively decreased the cellular level of CKB enzymatic activity (data not shown), as well as the abundance of CKB protein (Fig. 2A), and resulted in 60% reduction in the viral RNA level in SGR-N cells compared to the cells treated with control siRNA. This inhibitory effect of siRNA on HCV RNA abundance was also observed in JFH-1-derived subgenomic replicon (SGR-JFH1) cells. The viral RNA level in the cells transfected with siCKB-2 decreased by 50% compared to the control (Fig. 2A). We also tested the CKB mutant, CKB-C283S, in which Cys at aa 283, near the catalytic site, has been replaced with Ser (Fig. 3A) and which is known to be enzymatically inactive and to work in a dominant-negative manner (22, 29). As expected, overexpression of CKB-C283S resulted in a reduction in HCV RNA replication in SGR-N cells (Fig. 2B). We obtained a similar result in SGR-JFH1 cells, as described below (Fig. 3E).

To further examine the involvement of CKB in HCV RNA replication, we tested the effect of Ccr, a substrate analogue and possible inhibitor for CK in either SGR-N, SGR-JFH1 (Fig. 2C), or Huh7 cells transiently replicating luciferase-subgenomic replicon (data not shown). We found dose-dependent inhibition of HCV RNA replication but no observed effect on total cellular levels of protein and ATP (Fig. 2D) in the replicon setting used.

We next examined whether the knockdown of CKB or treatment with Ccr would abrogate the production of HCVcc. At 72 h posttransfection with siCKB-2, the HCV core level in cells infected with HCVcc was significantly reduced (Fig. 2E). Treatment of the infected cells with Ccr at various concentrations also reduced the intracellular and supernatant core level and subsequently decreased HCVcc production (Fig. 2F). These results demonstrate that suppression of the HCV RNA replication by the siRNA-mediated knockdown of CKB or treatment with CKB inhibitor leads to reduction of the production of infectious virus.

CKB interacts with HCV NS4A. Having established a role for CKB in HCV RNA replication, we then tried to determine to how CKB influences the HCV life cycle. It has been re-